uOttawa

L'Université canadienne
Canada's university

FACULTÉ DES ÉTUDES SUPÉRIEURES ET POSTOCTORALES

uOttawa

L'Université canadienne
Canada's university

FACULTY OF GRADUATE AND POSDOCTORAL STUDIES

Przemyslaw Mark Kwiecinski
AUTEUR DE LA THÈSE / AUTHOR OF THESIS

M.Sc. (Physics)
GRADE / DEGREE

Department of Physics
FACULTÉ, ÉCOLE, DÉPARTEMENT / FACULTY, SCHOOL, DEPARTMENT

Non Contact All Optical Thermal Conductivity Measurement Utilizing Raman Spectroscopy

TITRE DE LA THÈSE / TITLE OF THESIS

Dr. S. Desgreniers
DIRECTEUR (DIRECTRICE) DE LA THÈSE / THESIS SUPERVISOR

CO-DIRECTEUR (CO-DIRECTRICE) DE LA THÈSE / THESIS CO-SUPERVISOR

EXAMINATEURS (EXAMINATRICES) DE LA THÈSE / THESIS EXAMINERS

Dr. D. Rancourt

Dr. D. Rogers

Dr. H. Schriemer

Gary W. Slater
Le Doyen de la Faculté des études supérieures et postdoctorales / Dean of the Faculty of Graduate and Postdoctoral Studies

Non Contact All Optical Thermal Conductivity Measurement Utilizing Raman Spectroscopy

By
Przemyslaw Mark Kwiecinski
M.Sc. Thesis

Thesis submitted to the Faculty of Graduate and Postdoctoral Studies
of the University of Ottawa
In partial fulfillment of the requirements for the degree of
Master of Science

Department of Physics
University of Ottawa
Canada

Your file Votre référence
ISBN: 978-0-494-18433-2
Our file Notre référence
ISBN: 978-0-494-18433-2

Abstract

Original experimental data for the temperature dependence of the Raman shift in silicon and gallium sulfide is presented. An all optical thermal conductivity method, using an equation presented by Périchon *et al.*[2] and Nonnenmacher *et al.*[23], is applied to silicon and gallium sulfide. Theoretical calculations by Moody *et al.*[20] and Nissam *et al.*[22] are compared to the experimental results of Périchon *et al.* for the first time. The thermal conductivity of silicon is measured at 23 °C , 200 °C, and 300 °C, and of gallium sulfide at 23 °C. We investigate the possibility of measuring thermal conductivity at high pressures.

Preamble

Acknowledgement

I would like to thank my supervisor Professor Desgreniers for the countless hours spent aligning optics and explaining the subtleties of Raman spectroscopy. Your understanding and patience was the difference between my success and failure in this Master's degree. I would like to thank you for the time and energy spent revising and editing this thesis. None of this would be possible without your tireless effort and counsel.

I would like to thank my lab mates, Jesse Smith and Roxanna Flacau, as well as our perennial visitor Ryan Bolen. Your willingness to listen to me rant during times of frustration and brag during successes is greatly appreciated. Your friendship is valuable to me and I can only hope that wherever life may lead I find people like you there.

I would like to also thank the examiners, Professor Denis Rancourt, Professor Henry Schriemer, and Professor David Rogers for their time and effort in reading my thesis and commenting on the document.

Statement Of Originality

Original experimental data for the temperature dependence of the Raman shift in silicon and gallium sulfide is presented. An all optical thermal conductivity method, using an equation presented by Périchon *et al.*[2] and Nonnenmacher *et al.*[23], is applied to silicon and gallium sulfide. Theoretical calculations by Moody *et al.*[20] and Nissam *et al.*[22] are compared to the experimental results of Périchon *et al.* for the first time. The thermal conductivity of silicon is measured at 23 °C , 200 °C, and 300 °C, and of gallium sulfide at 23 °C. We investigate the possibility of measuring thermal conductivity at high pressures.

Table of Contents

List of Figures

Chapter 1: Introduction

1.1 Presentation of the Problem

Thermal conductivity is a basic property of any material. It is important in the study of heat transfer, electron and phonon mobility, as well as the strength and stiffness of the bond between atoms in a crystal. Thermal conductivity is the ratio between the energy flux through a material and its temperature gradient. It is commonly defined as the rate of heat transport within a material, meaning the amount of heat energy that passes through a volume of a substance for a unit of time per unit difference of temperature.[1] It has the units $\frac{J}{sm^2 K/m}$, which are generally condensed to $\frac{W}{m \bullet K}$. Thermal conductivity is affected by such factors as the temperature of the sample, the density of the sample, and changes with the phase of the material. Phase transitions can be identified by a sudden change in the material's thermal conductivity.

Conventional methods of measuring thermal conductivity include physically attaching a heat source and a heat sink to the sample. The heat propagates through the material and is detected at two points. Conventional methods require physical contact of the sensors and heaters to the sample, which introduces contact resistances. These degrade the quality of the data and limit the method's application. Eliminating the physical contact from the measurement would be a vast improvement on this method. A non contact method would not require any complicated sample preparation, and would be non invasive. This would allow the measurement to be done in more complicated environments required for high temperature and pressure conditions. We wish to develop

a thermal conductivity measurement method for solids that uses only laser light heating and an optical temperature probe, following the work of Périchon *et al.*[2] We refer to the method as an "all optical method".

A non-contact, all optical thermal conductivity method has many fundamental advantages over conventional contact measurement methods. First, it can be used on much smaller samples and in environments where physical contact is not possible. Secondly, it alleviates the problem of contact resistance which can degrade the quality of the results. This leads to a more versatile measurement method that should produce better quality results.

A thermal conductivity measurement requires a heating source, a heat sink, and a thermometer. For the all optical thermal conductivity method proposed in this thesis, a focused laser beam is used as the heating source. The sample itself, given its relatively large thickness, acts as the heat sink, and the sample temperature is detected through the Raman effect. Using these measurements the thermal conductivity of the sample is calculated.

1.2 Background and Literature Review

This research field was pioneered by an article written by McDonald and Wetsel[3] who analyzed the temperature rise in a material due to heating by a pulsed laser source. McDonald *et al.*[3] solved the heat equation for a general beam spot shape. This paper was referenced in articles by Lax,[4] and Cline *et al.*[5] Lax analyzed the temperature profile induced by a continuous wave laser beam onto a material. They used a temperature independent thermal conductivity in their calculations. This work was augmented by

Cline *et al.*[5], who analyzed the temperature field resulting from a moving, continuous wave laser during melting and cooling processes for heat treatment of metals.

Cline *et al.*'s work led to papers by Nissim *et al.*[22] and Moody *et al.*[20] The paper by Nissim *et al.*[22] focused on the temperature profile induced on the surface of a material by a continuous wave laser on the material, where the thermal conductivity is dependent on temperature. They solved the heat equation for a generic beam spot shape and a Gaussian beam profile. Moody *et al.*[20] extended the work by incorporating temperature dependent surface reflectivity into the calculations as well. Both papers developed a formula for the front surface temperature as a function of the absorbed incident laser light power.

The work of Cline *et al.*[5] was simplified by Nonnenmarcher *et al.*[23] They began with Cline *et al.* results for a moving laser beam, and simplified it to the special case of a stationary laser beam. The formula obtained was for the peak temperature rise of the material at the center of the beam spot, assuming no temperature dependence on the thermal conductivity and reflectivity. This formula was manipulated to determine the thermal conductivity of the material by knowing the absorbed incident power and the induced temperature at the center of the beam spot. The experiment performed by Nonnenmarcher *et al.*[23] utilized laser heating and a contact temperature measurement method.

The use of an all optical method for the measurement of thermal conductivity was continued by Périchon *et al.*[2] They used laser heating of the sample but utilized a Raman signal as a temperature probe. The experiment performed was an all optical thermal conductivity measurement conducted on porous silicon. Their data analysis was based on

the formula derived by Nonnenmarcher *et al.*[23] which will be reviewed in Chapter 4 of this thesis.

The all optical thermal conductivity measurement experiment performed by Périchon *et al.* and reproduced in this thesis and has two components. First the Raman shift's temperature dependence must be calibrated to give an all optical thermometer. The second part of the experiment is to measure the thermal conductivity by determining the temperature rise on a sample due to a known amount of laser heating.

1.3 Ultimate Goal of Our Research Problem

The ultimate goal of our research problem is to be able to determine the thermal conductivity of materials under high pressures and high temperatures. These materials can be investigated inside of the diamond anvil cell. Environmental conditions of interest achieved with the diamond anvil cell are pressures up to 500 GPa and temperatures up to 5000 K. These conditions mimic the temperature and pressure at the center of the Earth and giant planets of our solar system. To the knowledge of the author, no direct thermal conductivity measurements of dense and hot geomaterials have been made. Direct measurements of thermal conductivity values are important as they are used in models of Earth heat conduction. Currently only estimates for these values are available.

Inside of a diamond anvil cell a sample is placed between two diamonds. Under the extreme conditions stated above, direct physical contact with the sample is difficult. Inside the diamond anvil cell an all optical experiment is possible because of the transparency of the diamond to visible light. The all optical thermal conductivity method

suggested in this thesis can be used to measure the thermal conductivity of samples at extreme temperatures and pressures inside of the diamond anvil cell.

The specific goals for the current thesis are : (1) design and built the necessary instrumentation to carry out measurements of thermal conductivity using an all-optical method ; (2) calibrate the Raman shift 's temperature dependence of selected materials; (3) verify the method by performing measurements on selected materials at room conditions; (4) verify the method by performing measurements on selected materials as a function of elevated temperatures ; (5) draw conclusions regarding the usefulness of the proposed method for an eventual application to thermal conductivity measurements at extreme conditions.

1.4 Summary of What Has Been Achieved

The thermal conductivity of silicon and gallium sulfide (GaS) is measured using measurements of the absorbed incident laser light, the beam spot size and the temperature increase induced, as measured by Raman spectroscopy. Silicon is chosen as it is highly characterized, and gallium sulfide because of its strong Raman signal. The experimental thermal conductivity results of Périchon *et al.*[2] are compared to the theoretical results of Moody *et al.*[20] and Nissam *et al.*[22] and then validated.

Chapter 2: Phonon Spectrum of a Material

2.1 Introduction

The Raman scattering process must be understood to determine how it is used as a temperature sensor. A description of optical phonons is needed to understand the Raman effect. The atomic motion in a crystal is coordinated due to the periodicity of the arrangement. The motion of one atom affects the motion of the surrounding atoms, and the energy and momentum of this motion propagates away from it in a predictable manner. This coupled motion is referred to as a phonon. A phonon is also a quantum of vibrational energy. All the phonons inside of a material comprise its phonon spectrum, and this phonon spectrum changes with temperature. Optical phonons are caused by the relative motion of atoms relative to other atoms in the same unit cell.

2.2 The Crystal Lattice and Elastic Waves

A crystal is a material that exhibits long-range atomic order. It is an infinitely repeating periodic array of atoms or molecules.[6] The crystal can be reduced to two components: the basis, the unit that is infinitely repeated, and the lattice, the frame of the crystal that indicates the points in space where each base structural unit will attach.

The lattice is subdivided into identical unit cells. If the unit cell is applied in a repeating ordered fashion, this cell will fill the entire volume of the crystalline material.[6] A primitive unit cell is a minimum volume lattice cell, and the arrangement of atoms in it is the primitive basis. For instance, the primitive basis of the diamond structure is a face-centered cubic lattice, and contains two identical atoms located at (0,0,0) and

(¼, ¼, ¼), shown in Figure 2.1. This is the crystalline arrangement of silicon, germanium, and diamond.

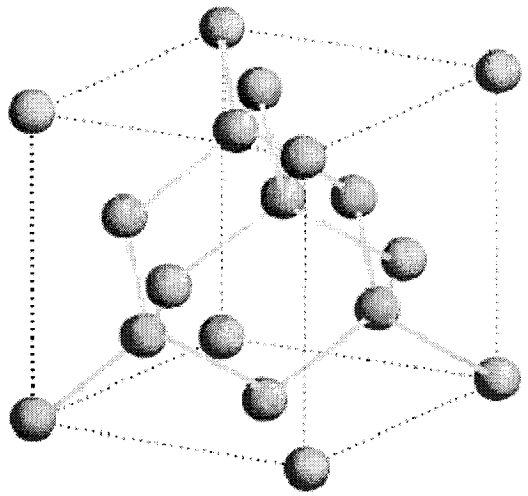

Figure 2.1 : The crystal structure of diamond. The lattice is a face-centered cubic, and the basis is two identical atoms at (0,0,0) and (¼, ¼, ¼). The conventional unit cube shown above contains eight atoms, and the primitive basis for the diamond structure contains 2 atoms. The grey solid lines between atoms indicate nearest neighbor bonds. Figure reproduced from Kittel. [6]

All atoms are constantly in motion. In a crystal lattice all atoms vibrate about a point of minimum energy.[7] As an atom moves, its nucleus and electronic distribution relative to nearby atoms are modified. This changes the electromagnetic forces between adjacent atoms. Nearby atoms feel this alteration in force and move to compensate.

The motion of one atom away from its minimum energy equilibrium point disturbs nearby atoms. They compensate by being pulled away from their old equilibrium points. The motion of the original atom thus propagates away from it in an ordered fashion. The surrounding atoms carry away the energy and momentum of the original displacement, allowing the original atom to fall back into its equilibrium state. This coupled motion is referred to as an elastic wave.

2.3 Elastic Waves Described as Phonons

Elastic waves in a crystal are treated by expanding each one into a Fourier series. The complete elastic wave is dissected into a series of standing elastic waves in the material referred to as normal modes. The mathematical description of the amplitude of a normal mode in one dimension is :

$$y(x,t) = A\sin(kx - \omega t) + B\cos(kx - \omega t)\,. \tag{2.1}$$

$\vec{k}$ is the wavevector and relates to the wavelength and direction of the vibration, and ω is the angular frequency and relates to the time evolution of the motion.[8] The elastic wave is comprised of a collection of normal modes, each with a unique angular frequency and wavevector. The energy in the elastic wave is also quantized, and this energy is divided among the various normal modes. A normal mode is completely described by stating that it has an angular frequency ω, wavevector $\vec{k}$, and n quanta of energy.

Normal modes are important because elastic wave collisions are described by an interaction of their normal modes. The normal modes are treated as particles, referred to as phonons. Rather than stating that a normal mode of wavevector $\vec{k}$, angular frequency ω and n quanta of energy exists, one states that n phonons exist each with wavevector $\vec{k}$ and angular frequency ω. The interaction of the original elastic wave is determined by summing up all the interactions of all the phonons that represent it. The time evolution of the original elastic wave is interpreted as particle creation, collision and absorption events.

2.4 Acoustic and Optical Phonons

Phonons are classified into optical and acoustic phonons. Acoustic phonons are caused by the relative motion of unit cells with respect to each other, and are considered as density fluctuations within a material. Optical phonons are the coordinated motion of atoms relative to each other within the same unit cell. For a material to contain optical phonons there must be at least two atoms contained within the unit cell.

2.5 Quantum Mechanical Description of a Phonon

Phonons also have a quantum mechanical description. In accordance with quantum mechanics the energy levels of a crystal lattice are quantized. The atoms in a crystal can be excited into higher vibrational modes. A phonon is a quantum of vibrational energy and represents the amount of energy needed to go from one vibrational mode to another. The phonon creation and annihilation operators cause the stationary state of the crystal lattice to increase or decrease in energy.

2.6 Phonon Dispersion Relationship of the Diamond Structure

A dispersion relationship can be developed between the wavevector, $\vec{k}$, of a phonon and its angular frequency ω. This relationship is of central importance in the study of phonon interactions. The dispersion relationship gives an understanding of the types of phonons in the material.

Silicon, the material considered in this thesis, at ambient temperature exists in a diamond structure. The dispersion relationship for the diamond structure is derived in Kittel.[6] All the significant independent magnitudes of the wavevector, $|\vec{k}|$, are found

between 0 and $\frac{\pi}{a}$ cm^{-1}, where a is the lattice constant of the unit cell. These wavevectors define the first Brillouin zone. At $\vec{k}$ = 0 cm^{-1}, there are two independent solutions, two branches, to the dispersion relationship:

$$\omega = 0 \quad (2.2) \quad \text{and} \quad \omega = \sqrt{\frac{4C}{M}} \,. \quad (2.3)$$

At the edge of the first Brillouin zone, at $|\vec{k}| = \frac{\pi}{a}$ cm^{-1}, there is only one solution:

$$\omega = \sqrt{\frac{2C}{M}}, \quad (2.4)$$

with C being the force constant between atoms and M being the mass of the atoms. These two branches of the dispersion curve describe two different types of phonons. The lower branch is referred to as the acoustic branch, as the frequency of zero at zero wavevector is an acoustic property. The second branch is the optical branch, having a frequency that is fundamentally independent of $\vec{k}$, and reaches a maximum at zero wavevector. Optical phonons are used in the experiment described in this thesis.

2.7 Importance of Phonons

Phonons are important because they provide information about the underlying structure of the material. The angular frequency and wavevector of a phonon is dependent on the elastic force constant between atoms. This force constant contains information about the atomic spacing, energy content, and various other qualities of the crystal.[9] As the temperature is changed, the distance and therefore the force constant between atoms also changes. The force constant is a measure of the temperature of the crystal, and

therefore phonons are a possible temperature probe of the material. One experimental method that provides information about the phonons inside a material is Raman spectroscopy.

Chapter 3 : Raman Scattering

3.1 Introduction

The Raman effect is caused by the scattering of a photon with a phonon, with the subsequent emission of an energy shifted photon. The Raman signal is a measure of the frequency of the optical phonons near the center of the first Brillouin zone in a material. The peak frequency of the Raman signal changes with temperature. The Raman signal can therefore be used as an optical thermometer.

3.2 Optical Processes

In a crystal, the charge carriers such as electrons and nuclei are bound together in the crystal lattice. As an electromagnetic wave enters the material, a sinusoidal varying electric field is felt by the atoms. This causes the electrons to react, and the atoms form oscillating dipoles. This is referred to as an induced polarization. The equation relating the induced polarization to the applied electric field inside of a material is shown below[10]:

$$P = X_1 \varepsilon_0 E + X_2 \varepsilon_0 E^2 + X_3 \varepsilon_0 E^3 \ , \qquad (3.1)$$

with P being the polarization, X_1 the linear susceptibility, X_2 and X_3 the nonlinear susceptibilities, ε_0 the permittivity of a vacuum, and E the electric field. Equation 3.1 defines the interactions of light with matter. An optical process is a linear optical effect if the first order term of Equation 3.1 dominates the polarization, and it is nonlinear if the higher order terms dominate.

Linear optical effects occur at low light intensities from sources such as a flashlight or direct sunlight. At low light levels, the induced polarization is linearly

dependent on the strength of the input electric field. The optical properties of materials are not affected by the intensity of light. Linear interactions are all single photon events governed by the X_1 term in Equation 3.1, and include processes such as superposition, reflection, refraction, and absorption.

Nonlinear optical effects result from the second or higher order terms in Equation 3.1. At very high electric field strengths the polarization produced within the material is no longer proportional to the inner field strength. When the electric field intensity caused by light is near 10^5 V/m^2, the intensity of the field is comparable to the binding energy of the electron.[10] The material properties change with the intensity of light, and the effect is nonlinear. Nonlinear optical effects are the result of two or more photon interactions. These processes are broadly divided into the categories of parametric processes and inelastic processes.

During a parametric process the material passively responds to the incident light. The material can be considered inactive with its nuclei remaining fixed. The resulting effects are due to the input electric field existing inside the material.[7] Some examples of these are sum and difference frequency generation and second harmonic generation, which both interact through the quadratic term in Equation 3.1 .[11] Another example is Rayleigh scattering, in which light is absorbed by the medium then reradiated out at the same wavelength.

During an inelastic process, the medium is an active part of the interaction. The instantaneous motion of the atom is taken into account and changes the optical response of the material.[7] This results in energy being transferred between the material and the optical wave, and involves three or more waves. One example of an inelastic process is

Raman scattering. Raman scattering provides information about the phonons in a material.

3.3 Raman Scattering

In Raman scattering, incident photons interact with optical phonons and a photon is emitted. Optical phonons are the result of coordinated atomic vibrations within the crystal lattice,[12] and are due mainly to thermal effects.[7] Compared to elastic Rayleigh scattering, the intensity of the Raman effect is quite small. Rayleigh scattering occurs once for every 10^3 photons that are incident on the material.[7] The Raman effect occurs once for every 10^6 incident photons, and its intensity is proportional to the fourth power of the frequency of the irradiation.[13] [14] In designing an experiment, the highest frequency of incident laser light that is practical is used.

As an atomic nucleus moves in response to thermal motion, its electron distribution also moves. Its nucleus is now closer to an adjacent nucleus, and their electron clouds move in opposite directions to compensate, altering their polarization. This causes the next atom's electron cloud to compensate and the disturbance propagates through the material. In this fashion the motion of the original atom propagates through the material, forming a wave which defines a phonon.

Optical phonons can interact with photons and other phonons. These phonons carry energy and crystal momentum through the material. The conservation equations that govern this transport are shown as follows[7] :

$$h\omega' = h\omega \pm h\omega_s(k) \tag{3.2}$$

$$h\vec{q}' = h\vec{q} \pm h\vec{k} + h\vec{G} \tag{3.3}$$

where ω', $\vec{q}'$ are the frequency and wavevector of the emitted photon, ω, $\vec{q}$ are the angular frequency and wavevector of the absorbed photon, ω_s, $\vec{k}$ are the angular frequency and wavevector of the annihilated or created phonon, and $\vec{G}$ is a reciprocal lattice vector. During the Raman effect, optical phonons are either created or destroyed. By measuring the frequency of the incident and scattered light from a sample, the frequency of the phonon involved in the process can be calculated.

A key to this technique is that the wavevectors of photons are on the order of 10^5 cm^{-1}, and the first Brillouin zone is on the order of 10^8 cm^{-1}. This implies that to conserve momentum, photons can only interact with phonons near the center of the first Brillouin zone in the neighborhood of $\vec{k} \sim 0$.[7] This is advantageous for two reasons. The first is that acoustic phonons in this region have nearly zero energy and cause no shift, resulting in us only dealing with optical phonons. The second is that at the center of the Brillouin zone, optical phonons cause a large frequency shift that is fairly constant over a range of k near the origin.

Equation 3.2 describes two processes. The first is the creation of a phonon and the production a photon of lower frequency. This is the Stokes component of the emitted light. The second is the absorption of a phonon and the production of a photon of higher frequency. This is the anti-Stokes portion of the scattered light.[7] Symmetrically around the laser line excitation is the Stokes line, found at longer wavelengths, and the anti-Stokes line, found at shorter wavelengths.

3.4 Quantum Mechanical Description of the Raman Effect

In quantum mechanics, phonons are considered as quanta of vibrational energy that raise or lower the energy level of the crystal lattice. In perturbation theory, the Raman effect is the absorption or creation of a phonon via a virtual energy state. The system begins at an initial vibrational energy level (VEL A). A photon is absorbed by the system and raises the lattice to a virtual energy level. The system falls back down to a final vibrational energy level (VEL B) through the emission of a photon.

The two vibrational energy levels do not have to be equal in energy. If VEL B is of higher energy than VEL A, energy has been absorbed by the system. A phonon has been created and the energy of the scattered photon is lower then the incident photon. This is Stokes scattering. If VEL B is lower then VEL A the system has lost energy, a phonon has been annihilated and the photon energy has been shifted higher. This is anti-Stokes scattering. If VEL B is equal to VEL A the photon's energy remains the same and this is Rayleigh scattering. This is shown in Figure 3.1.

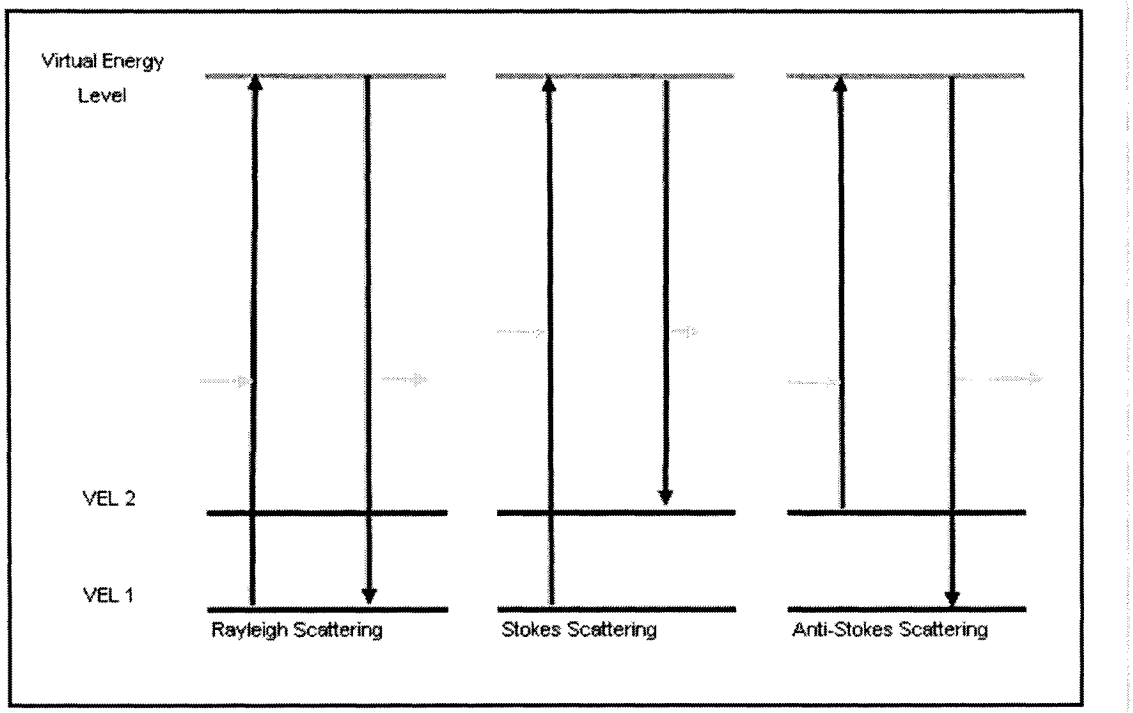

Figure 3.1 : The quantum mechanical description of the Raman effect. The black arrows show the changes in the energy levels that the system undergoes. The grey arrows represent photons, with the length of the arrow corresponding to the relative energy and frequency of the photon. The system absorbs a photon and is raised to a virtual energy level. The system then falls back to a lower energy level through the emission of a photon (horizontal arrows). If the final energy level of the system is equal to the initial energy level of the system, then Rayleigh scattering has occurred and the emitted photon is equal in energy to the absorbed photon. If the final energy level is higher in energy than the initial energy level then Stokes scattering has occurred. A phonon is created and the photon's energy has been reduced. If the final energy is lower than the initial energy of the system then anti-Stokes scattering has occurred. A phonon has been annihilated and the emitted photon has higher energy and frequency than the absorbed photon.

3.5 The First Order Raman Spectrum

The dispersion relationship for diamond materials probed by the Raman shift is shown below:

$$\omega = \sqrt{\frac{4C}{M}}\,. \tag{3.4}$$

The frequency of these phonons is not constant. A change in the force constant C changes the frequency of the optical phonons near the center of the Brillouin zone, and therefore

changes the Raman shift. Raman spectroscopy therefore provides information about the interatomic restoring forces which exist in the crystalline material.

The bond lengths within the crystal relates to this restoring force. As the temperature of a material increases, the material expands and the spacing between atoms increases. As the material expands the forces between atoms are diminished and the spring constant is lowered. This leads to a lower frequency shift in the Raman spectrum. This is published in the literature for dispersed oxides,[15] semiconductors,[16] and a large array of other materials.[17 18]

Increasing the temperature also leads to peak broadening. Thermal expansion of the crystal lattice causes the decrease in the intensity of the Raman peak. The frequency shift is proportional to the force constant between atoms, which is related to their average distance from each other. At higher temperatures, the atoms have a broader range of possible distances between them and therefore possible force constants. This leads to the Raman peak broadening. The total integrated intensity of the peak remains the same, but the intensity at the center of the peak is reduced as the temperature is increased.

3.6 Comparison of The Dispersion Curves of Diamond Materials

The first order Raman shift of various materials with the diamond structure can be compared by simply referring to their dispersion relations, $\omega = \sqrt{\frac{4C}{M}}$. The mass of a silicon atom is more than two times greater than that of a carbon atom. The bonds of diamond are much stiffer and have a much higher force constant than those of silicon. These two factors combine to produce a much smaller Raman shift for silicon than for

diamond. At room temperature the approximate Raman shift of diamond is 1331 cm^{-1} [19] and for silicon it is 520 cm^{-1}. [2]

3.7 Conclusion

The Raman signal is dependent on the force constant between atoms. As the sample is heated, this force constant changes, and this change can be seen in the shift of the Raman signal. The Raman signal can therefore be used to measure the temperature change of a sample.

Chapter 4 : Integration of the Heat Equation to Obtain the Thermal Conductivity

4.1 Introduction

The heat equation was solved separately by Moody *et al.*[20] and Cline *et al.*[5] to give two separate equations for the local temperature rise of a material due to induced laser heating. These two equations were then separately manipulated to give two equations for the thermal conductivity of a material. The first equation was derived by Moody *et al.*[20] taking into account the temperature dependence of the thermal conductivity and the reflectivity, and is given by Equation 4.20. The formula derived by Moody *et al.*[20] has more realistic assumptions, but is not very convenient as it requires knowledge of the thermal conductivity temperature dependence to calculate the thermal conductivity. A second equation was independently derived by Cline *et al.*[5] , under the assumption that the thermal conductivity and reflectivity are temperature independent, and is shown in Equation 4.28. The formula derived by Cline *et al.*[5] was used by Périchon *et al.*[2] during his all optical thermal conductivity experiment.

4.2 Thermal Conductivity Equation Derived by Moody and Co-workers

By knowing the amount of energy being absorbed by the sample, the sample's front surface temperature rise, and the laser spot size, Moody *et al.* [20] found the thermal conductivity from the heat equation:

$$\frac{\partial T}{\partial t} - D\nabla^2 T = \frac{Q}{C_p}, \tag{4.1}$$

where D is the thermal diffusivity, Q is the input energy, and C_p is the specific heat of the material, and T is the temperature. The quantity $D\ C_p$ is equivalent to the thermal conductivity, K.

4.3 The Input Energy Into the Sample

The input energy into the sample, Q, is the amount of laser light absorbed by the sample. The amount of energy absorbed is dependent on the beam intensity distribution and the amount of that incident laser energy actually absorbed by the sample. If the beam is assumed to have a Gaussian intensity distribution, the amount of energy incident on the sample at position (x,y,z) is:

$$I(x,y,z) = I_o \exp\left(\frac{-2x^2}{r^2}\right)\exp\left(\frac{-2y^2}{r^2}\right)\delta(z) \quad , \tag{4.2}$$

with I_o being the peak intensity, r is the radius of the beam, x and y are coordinates in a plane perpendicular to the beam, and z is a coordinate parallel to the beam. The delta function $\delta(z)$ is used to indicate that all the input energy is absorbed at the surface at $z = 0$. The peak intensity corresponds to :

$$I_o = \frac{2P}{\pi r^2}, \tag{4.3}$$

where P is the total incident power. The input energy into the system is the amount of incident energy absorbed by the sample, Q:

$$Q(x,y,z) = IA = \frac{2PA}{\pi r^2}\exp\left(\frac{-2x^2}{r^2}\right)\exp\left(\frac{-2y^2}{r^2}\right)\delta(z) \ , \tag{4.4}$$

where A is the absorbance, the ratio of the absorbed laser power to the incident power.

4.4 Calculating the Laser Light Absorbance

As seen in Equation 4.4, a parameter needed to calculate the input energy is the amount of the incident light absorbed by the sample and converted into heat. This is found indirectly by measuring the incident laser light, and then performing a theoretical calculation to determine what percentage of that light the sample will absorb as heat. There are three possible processes that occur when light is incident on a sample that are important for this experiment. The first is light reflecting and scattering off the front surface of the material. The second is transmission, when light passes through the entire sample volume without being absorbed. This only occurs with very thin films of semiconductors and metals, or thick dielectrics, and therefore is not a concern. The third is absorption, in which the light is converted to heat in the material. These are summarized in Equation 4.5 :

$$1 = R + T + A \ , \tag{4.5}$$

with R being the fraction of reflected light, T the fraction of transmitted light and A the fraction absorbed and converted to heat. Assuming that none of the light is transmitted, the equation becomes :

$$A = 1 - R \ . \tag{4.6}$$

Equation 4.6 is used to determine the proportion of incident light absorbed by the sample by Périchon *et al.*,[2] and McDonald *et al.*[3]. The reflectivity of a semiconducting material is determined by its index of refraction, n, and its extinction coefficient, k, through the following equation :

$$R^2 = \frac{(n-1)^2 + k}{(n+1)^2 + k} . \tag{4.7}$$

The index of refraction and the extinction coefficient change with the wavelength of the incident light. These coefficients are widely available and have been compiled into charts. The values for the reflectance of silicon at 21 °C are 37.4 % at 532 nm, 38.3 % at 514 nm and 39.6 % at 488 nm.[21] The reflectance is dependent on the sample temperature, sample surface roughness, and the incident angle of the laser light. Under the conditions used in this experiment, a sample with a polished surface and a laser beam at normal incidence, the material's reflectance was considered constant over the temperature range induced by the heating laser. By substituting Equation 4.6 into Equation 4.4, the input energy becomes :

$$Q(x,y,z) = \frac{2P(1-R)}{\pi r^2}\exp\left(\frac{-2x^2}{r^2}\right)\exp\left(\frac{-2y^2}{r^2}\right)\delta(z)\ . \tag{4.8}$$

4.5 Solution to the Heat Equation :

The heat equation, Equation 4.1 was solved by Moody *et al.*[20] by introducing a linearized temperature θ as shown in Equation 4.9:

$$\theta = \int_{T_s}^{T} \frac{K(T)}{K(T_s)} dT\,, \tag{4.9}$$

with $K(T_s)$ being the thermal conductivity of the sample at its bulk temperature, and $K(T)$ being the thermal conductivity of the sample at the localized heated temperature. The temperature profile induced by a continuous laser beam is the steady state time independent heat equation. Substituting the incident absorbed power, Equation 4.4, and the definition for linearized temperature, Equation 4.9, into the time independent heat equation one obtains :

$$\nabla^2\theta(x,y,z) = \frac{\left[\frac{2P(1-R)}{\pi r^2}\right]\exp\left(\frac{-2x^2}{r^2}\right)\exp\left(\frac{-2y^2}{r^2}\right)\delta(z)}{D(T)C_p(T)}. \tag{4.10}$$

The above equation was solved by Moody *et al.* [20] and Nissim *et al.*[22] to give

$$\theta(X,Y,Z) = \frac{2P(1-R)}{K(T)r}\frac{1}{\pi^{3/2}}\int_0^\infty \frac{1}{\left[(u^2+1)(u^2+\beta^2)\right]^{1/2}}\exp -\frac{1}{2}\left(\left(\frac{X^2}{u^2+1}\right)+\left(\frac{Y^2}{u^2+\beta^2}\right)+\left(\frac{Z^2}{u^2}\right)\right)du, \tag{4.11}$$

which uses the definition of thermal conductivity:

$$K(T) = D(T)C_p(T), \tag{4.12}$$

and the transformations $X = \frac{x}{r}, Y = \frac{y}{r}, Z = \frac{z}{r}$ to achieve dimensionless numbers. β is the eccentricity of the beam spot, which normalizes the radii of various spot geometries into a dimensionless number :

$$\beta = \frac{r_y}{r_x}. \tag{4.13}$$

At the center of the beam, with $X = Y = Z = 0$, the maximum temperature at the surface is achieved. By using these conditions the peak surface temperature is calculated. For a circular laser beam, the eccentricity β = 1. The linearized temperature, given by Equation 4.11, is then simplified and becomes:

$$\theta = \frac{2P(1-R)}{K(T)r}\frac{1}{\pi^{\frac{3}{2}}}\int_0^\infty \frac{1}{u^2+1}du, \tag{4.14}$$

$$\theta = \frac{2P(1-R)}{K(T)d}\frac{1}{\sqrt{\pi}}. \tag{4.15}$$

4.6 Linearized Temperature :

The front surface temperature is solved by incorporating the definition of the linearized temperature, Equation 4.9, into Equation 4.15. The temperature dependence of the thermal conductivity is modeled with the following inverse temperature relationship:[22]

$$K(T) = \frac{F}{(T - T_k)}, \tag{4.16}$$

where T is the front surface temperature in Kelvin, T_k is equal to 99 K for silicon and F = 299 W/cm for silicon. By substituting the inverse temperature relationship into the Equation 4.9, the linearized temperature becomes:

$$\theta = (T_s - T_k)\ln\left[\frac{T - T_k}{T_s - T_k}\right], \tag{4.17}$$

$$T = T_k + (T_s - T_k)\exp\left[\frac{\theta}{T_s - T_k}\right], \tag{4.18}$$

$$T = T_k + (T_s - T_k)\exp\left[\frac{K(T)\theta}{F}\right], \tag{4.19}$$

with T_s being the substrate temperature, and T being the peak surface temperature. When combined with Equation 4.15, this reduced to :

$$T = T_k + (T_s - T_k)\exp\left[\frac{P(1-R)}{2Fr\sqrt{\pi}}\right]. \tag{4.20}$$

Equation 4.20 is shown in Figure 4.1, and is given support from the paper by Périchon *et al.*[2] They measured the thermal conductivity of porous silicon at elevated temperatures. Périchon *et al.*[2] were able to achieve a surface temperature increase of 125°C, with a bulk temperature of 500°C and a laser spot diameter of 5 μm. Under these

experimental conditions, the measured temperature increase is predicted accurately by Equation 4.20. This provides support for the derivation of Moody *et al.*[20]

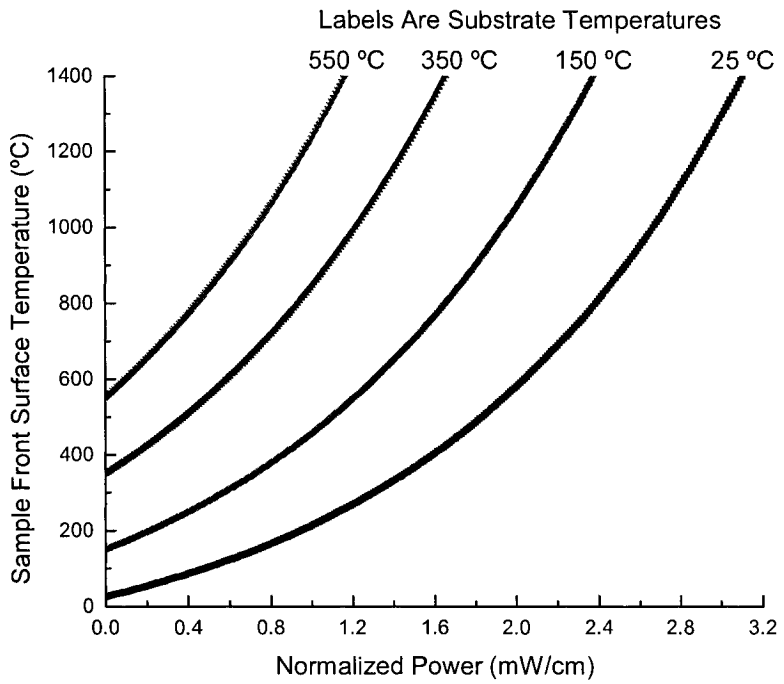

Figure 4.1 : The peak surface temperature rise of a sample irradiated by a Gaussian laser beam profile, computed from Equation 4.20. Each curve corresponds to a different bulk sample temperature, as indicated. Normalized power is the power delivered to the sample divided by the radius of the laser spot.

4.7 Thermal Conductivity Equation Derived by Cline and Co-workers

The equation used by Périchon *et al.*[2] was deduced by Cline *et al.* [5] With the assumptions of constant thermal conductivity, constant reflectivity, and a circular beam spot, Cline *et al.* found the thermal conductivity from the heat equation.

$$\frac{\partial T}{\partial t} - D\nabla^2 T = \frac{Q}{C_p} \quad . \tag{4.21}$$

With the notation being identical to the derivation carried out in the previous section. Once again assuming a Gaussian incident beam spot, the input energy is

$$Q(x,y,z) = IA = \frac{2PA}{\pi r^2}\exp\left(\frac{-2x^2}{r^2}\right)\exp\left(\frac{-2y^2}{r^2}\right)\delta(z)\ . \tag{4.22}$$

Cline *et al.* investigated the temperature rise on the surface of a material by a laser beam moving at a velocity of v. This changes the expression of the input energy into the material to :

$$Q(x,y,z) = \frac{[2P(1-R)]\exp\left(-\left[\frac{-2(x-vt)^2+2y^2}{r^2}\right]\left[2r^2\right]^{-1}\right)\delta(z)}{\pi r^2}. \tag{4.23}$$

The temperature rise at a point is found by integrating :

$$\Delta T(x',y',z') = \int_{-\infty}^{t}\int_{-\infty}^{\infty}\int_{-\infty}^{\infty}\int_{-\infty}^{\infty}(Q/C_p)(x'y'z't')\times G(x'y'z't'|xyzt)dz'dy'dx'dt' \ , \tag{4.24}$$

where G is a Green's function, and x', y', z', t', being the new local coordinates on the material. According to Cline *et al.* the Green's function for the diffusion equation at the surface becomes

$$G = \frac{\exp\left(-r^2\left[4D(t-t')\right]^{-1}\right)}{4\left[\pi D(t-t')\right]^{3/2}} \ , \tag{4.25}$$

where $r^2 = (x-x')^2 + (y-y')^2 + (z-z')^2$. At the surface, $z' = 0$, and time $t = 0$ the temperature is found to be

$$\Delta T(x,y,z) = \frac{[2P(1-R)]}{C_p}\int_0^{\infty}\frac{\exp\left[-\left\{(x+vt')^2 + y^2\left[2r^2+4Dt'\right)^{-1} + (z^2)(4Dt')^{-1}\right\}\right]}{(\pi^3 Dt')^{1/2}(2r^2+4Dt')}dt' . \tag{4.26}$$

Under the assumption that we are only interested in the very center of the beam, this reduces to

$$\Delta T = \frac{2P(1-R)}{C_p D \pi d} \exp\left(\frac{-v}{2D(r+x)}\right). \tag{4.27}$$

In the limit of zero velocity, meaning a stationary laser beam, the peak surface temperature rise at the center of the beam becomes :

$$\Delta T = \frac{2P(1-R)}{Kd}\frac{1}{\pi}. \tag{4.28}$$

Equation 4.28 was used successfully by Périchon *et al.*[2] to calculate the thermal conductivity of silicon from an all optical thermal conductivity measurement.

4.8 Equation Used To Analyze Experimental Data

Equation 4.28 requires values for the amount of light incident on the sample and the surface temperature rise. Thus an additional relationship is required to connect the experimental data with Equation 4.28. The first part of the all optical thermal conductivity experiment yields the Raman shift's temperature dependence (S_{Temp}), and the second part of the experiment yields the change in the Raman shift with incident laser heating (S_{Heat}). These two factors taken together give :

$$\frac{S_{Temp}}{S_{Heat}} = \frac{\left(\frac{Raman_{shift}}{\Delta T}\right)}{\left(\frac{Raman_{shift}}{P}\right)} = \frac{P}{\Delta T}. \tag{4.29}$$

Therefore Equation 4.28 becomes :

$$K = \frac{2P(1-R)}{\pi d \Delta T} = \frac{2(1-R)}{\pi d}\frac{S_{temp}}{S_{Heat}}. \tag{4.30}$$

This is the equation that is used to analyze the data collected.

4.9 Conclusion

Several assumptions are incorporated into Equation 4.30. The first is that the laser beam is at a normal angle to the sample. The second is that the surface of the sample is well polished. These two conditions were met by our experiment. If the incident beam angle is something other than 90°, the incident laser spot is elliptical. That increases the spot size from that of a circle and the temperature rise at the center of the laser spot is smaller. If the sample surface is not polished more light scatters off of the sample. As a result less incident light is being absorbed by the sample. Both of these conditions lead to a smaller temperature rise in the sample. The laboratory set up used in the experiment does all that is possible to have the largest temperature increase possible, as well as to measure it accurately.

Chapter 5: Working Principles of the Experimental Set-up

5.1 Experimental Optical Path

The optical path of the experimental setup is shown in Figure 5.1. The equipment and working principles are next described in detail, as well as the conditions under which the experiment took place. The laser light first travels through a monochromating filter, glass optics, then into a multimode optical fiber. It is then filtered by a laser line filter before entering a microscope configured to the 180° backscattering geometry. The light enters a beam splitter and then is focused on the sample by a microscope objective. The scattered light is collected by the same optics, passes through the beam splitter, is filtered by an edge filter, and goes through an output multimode fiber before entering a spectrograph. The scattered light enters through the entrance slit, is dispersed by the diffraction grating and is then measured by a CCD detector. It is possible to divert the scattered light onto a camera with the use of a moveable mirror, for visible inspection or laser beam profiling. Silicon and gallium sulfide are the chosen samples. Gallium sulfide has a layered structure which, as discussed later, affects the measured thermal conductivity.

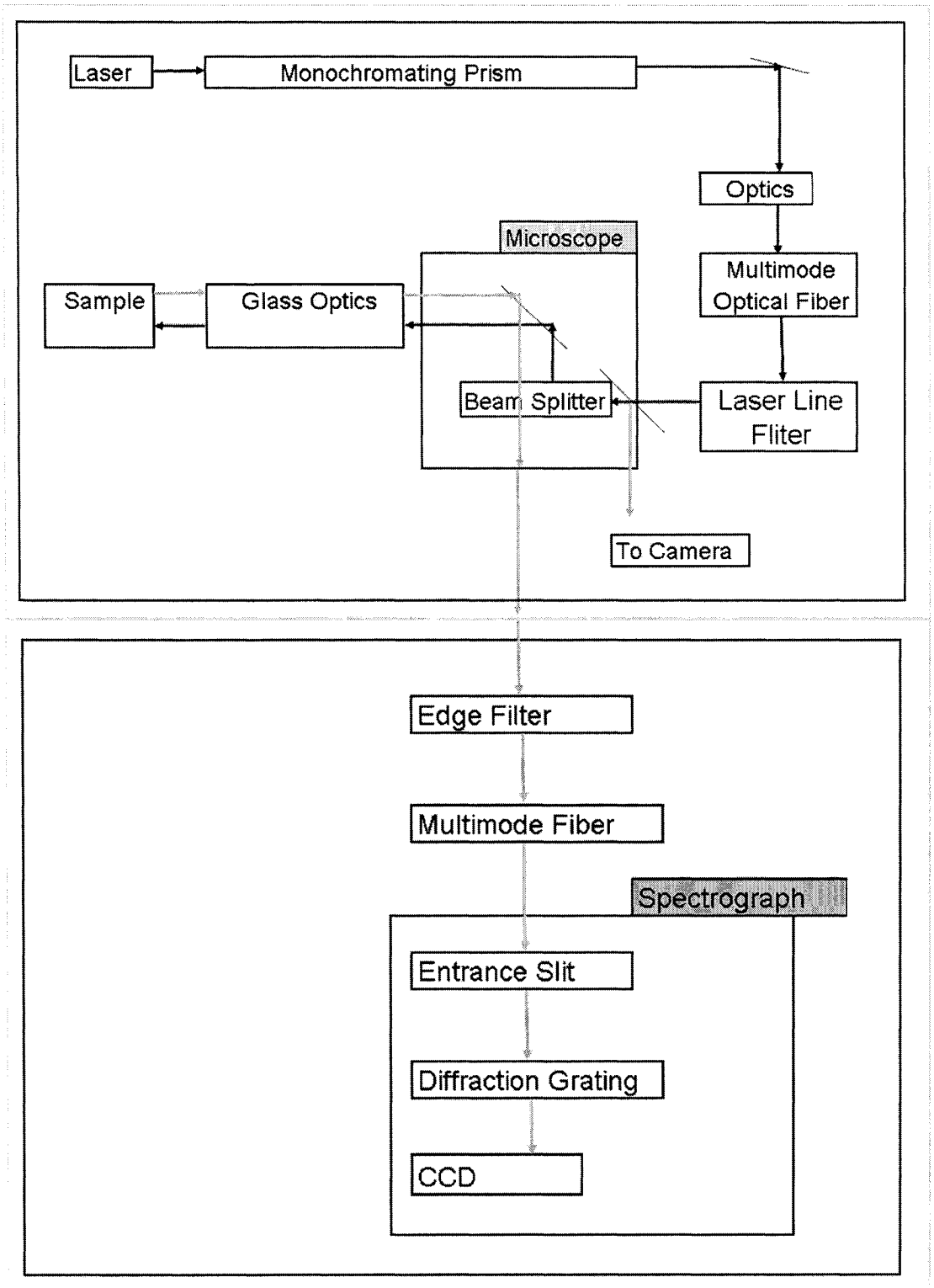

Figure 5.1 Schematic diagram of the optical path followed by the laser light. The laser light is shown in black arrows and the scattered light in grey arrows. The laser, microscope and spectrograph components of the optical setup are clearly shown. The setup is typical of a Raman spectroscopy experiment.

5.2 Justification of the Experimental Layout

The experiment involves conducting a thermal conductivity measurement by heating a sample with incident laser light and determining the temperature increase through the Raman shift. Raman spectroscopy plays a central role in the experiment, and as such the layout chosen for the experiment follows a typical Raman spectroscopy set-up. This includes laser light in the visible range, edge and laser line filters, as well as a liquid nitrogen cooled silicon detector. The 180° backscattered geometry is chosen because the samples used are not transparent to visible light.

5.3 Laser Light Excitation Sources

The laser used for 488 nm and 514 nm excitation is a Model 95 Ion Laser, sold by Lexel Laser, Inc.[23] It is a argon gas ion laser, with a 25 A power supply and cooled with a continuous flow water-jacket. Inside the housing argon is ionized and emits a range of wavelengths. The laser used for 532 nm excitation is the Centennia TD5 Thin Disk Laser sold by Spectra-Physics. It is a diode pumped solid state laser and operates at up to 5 W of continuous wave output power.[24]

The laser light is filtered upon exiting the laser. Photons of undesired wavelengths are present in the beam and must be removed. This is accomplished with the use of a monochromating filter which physically disperses the light to isolate the needed wavelength.

5.4 Optical Fibers

Upon exiting the monochromator, the light enters a fiber optic cable. The fiber optic used is the Thorlabs Step Index Multimode 0.22NA AFS50 Fiber Patch Cable with a useful spectral transmission range from 400 nm to 2400 nm [25] and a core fiber diameter of 50 μm. The attenuation spectrum is shown below in Figure 5.2. For the wavelengths used in the present work the transmission in the fiber is better than 99.9 % per meter.

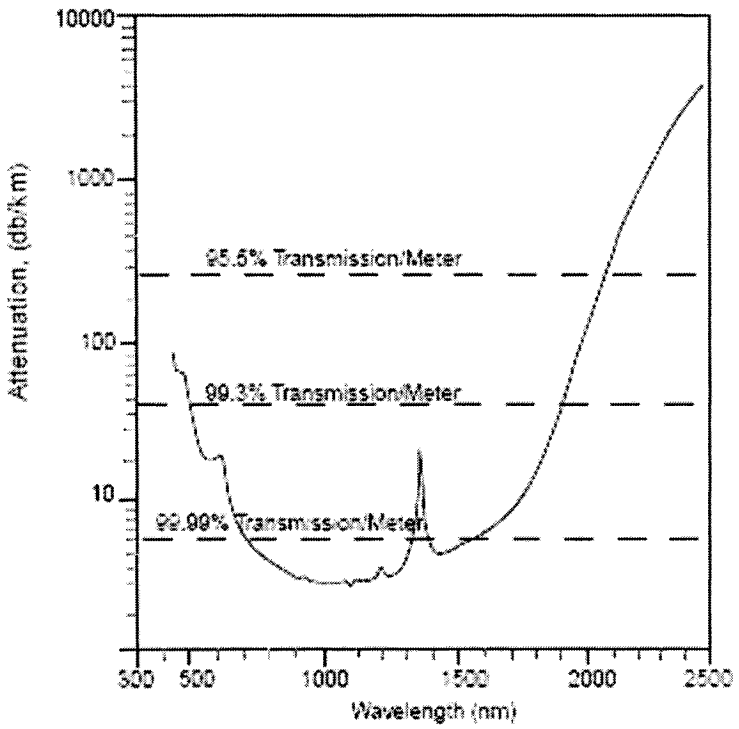

Figure 5.2 : The amount of light attenuated by the step index multimode patch cable for the wavelength range of 300 nm to 2500 nm. With the wavelengths of 488, 514 and 532 nm used in this experiment, the transmission through the fiber is approximately 99% per meter. Reproduced from the Thorlabs catalog.[26]

One complication with the use of the optical fiber is that both luminescence and a Raman signal from the glass are induced in the fiber by the propagating laser light. An

XLK06 laser line filter sold by Omega is used directly after the fiber optic to remove all incoming light except the 488 nm laser line. It has a diameter of 25 mm and a transmission full-width-half-maximum (FWHM) of 1.9 nm. The transmission spectrum of the laser line filter is shown in Figure 5.3 .

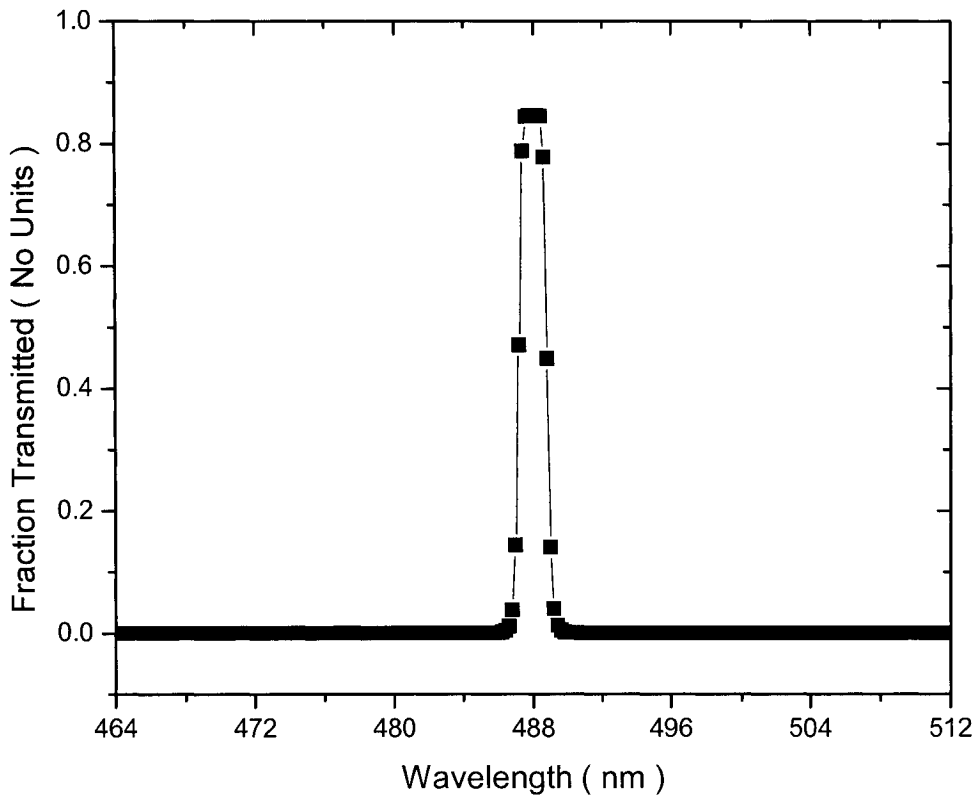

Figure 5.3 : Transmission spectrum of the 488 nm XLK06 laser line filter sold by Omega.[27] The peak shown is centered at 488 nm. The transmission of the laser line through the filter is 85 %.

The main advantage of optical fibers is that they are flexible. They can be adjusted into circular and spiral paths, and the position of the input and output ends can be easily and independently adjusted. The optical fiber can then be securely mounted. In this experiment, one end is fixed in place to capture the laser light directly after the

monochromator, and the other end is secured inside a microscope assembly. The microscope can then be adjusted without fear of misaligning the input laser beam.

5.5 Microscope at a 180° Backscattering Geometry

As the samples under investigation are opaque to light in the visible range, the 180° backscattering geometry is used. The light enters the microscope and passes through a 50/50 beam splitter. The beam splitter allows 50% of the light to propagate through and deflects the remaining 50% in the perpendicular direction. The deflected light strikes a tiltable 45° mirror then hits the sample and scatters off the surface back toward the microscope. A portion of this scattered light re-enters the microscope and propagates toward the beam splitter. 50% of the scattered light is transmitted through the beam splitter, perpendicular to the original direction of the beam. A beam splitter must be used in the 180° backscattering geometry so that the directions of the incoming and the scattered light are different. That way it is possible to divert the scattered light to the spectrograph. If a mirror were used the scattered light would simply follow the incident light's optical path back to the laser.

The main disadvantage of the 180° backscattering geometry is primarily the use of a beam splitter. A significant portion of the incoming light and the produced signal are lost. The advantages of the 180° backscattering geometry are its simplicity and cost efficiency, as the same optics are used for both the incoming and the scattered light. This simplicity also assures that both the laser spot and image are in focus relative to each other.

The signal produced by the sample is a combination of Raman and elastically scattered light. Upon the signal exiting the microscope, a 488nm XR3000 Vivid Standard edge filter sold by Omega Optical, is used to filter out the Rayleigh scattering from the signal. It has an 85% transmission average in the passband, and goes from an attenuation of 5 OD to 0.3 OD at 200 cm^{-1} from the laser line. This ensures that only the Raman scattered light will enter into the spectrometer. A transmission spectrum for the 488 nm edge filter is shown in Figure 5.4. The transmission spectrum for a 532 nm filter would be similar.

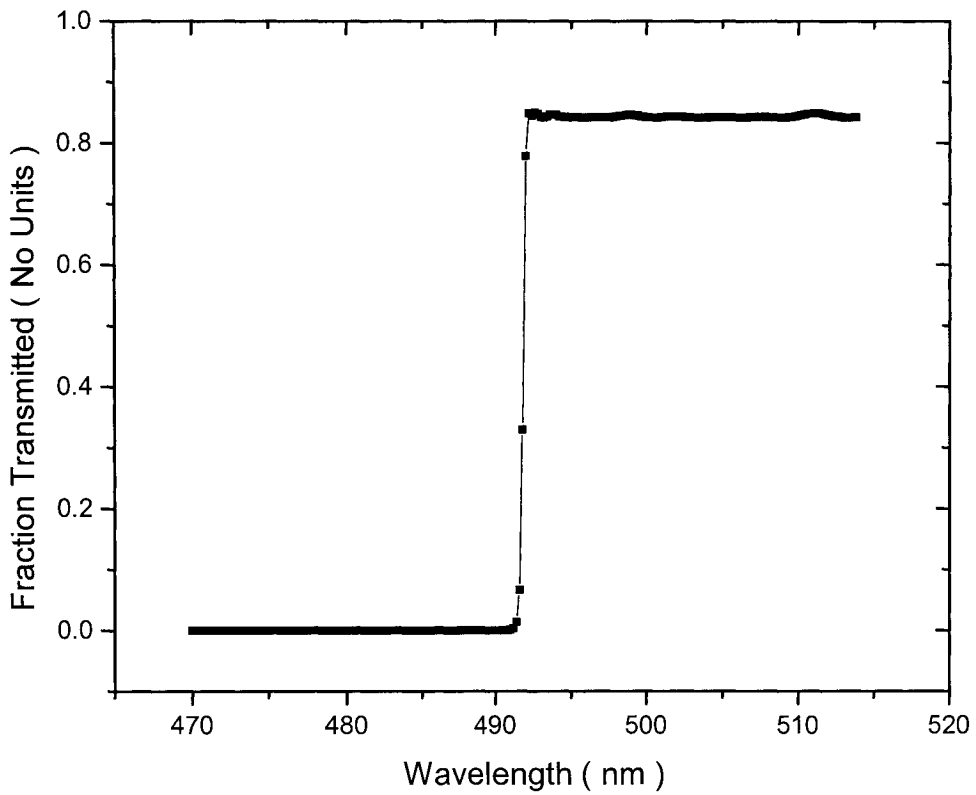

Figure 5.4 : Transmission spectrum of the 488 nm VIS Edge Filter by Omega Filters.[28] After the edge, transmission through the filter is near 85 %.

5.6 The Spectrograph Assembly

The scattered light travels through a second 200 μm diameter Thorlabs Step Index Multimode 0.22NA AFS200 Fiber Patch Cable before being focused onto the entrance slit of a spectrograph. The spectrograph is a Model FHR 640 Spectrometer produced by Jobin Yvon.[29] The spectrograph has a focal length of 640 mm with an entrance aperture ratio of f/5.4, and a spectral resolution of 0.016 nm assuming a 10 μm slit. The typical slit width used ranges from 5 μm to 30 μm.

Inside the spectrograph the light enters a light-tight housing and is incident upon a mirror at 45°, which reflects the light to a parabolic mirror. The parabolic mirror focuses the light at infinity and directs it toward the diffraction grating. The scattered rays are sent onto a second concave mirror and the spatially dispersed light is focused onto the detector plane.

The detector utilized is a liquid nitrogen cooled Spectrum One Charge Coupled Device (CCD), sold by Jobin Yvon Optical Spectroscopy Division. It is cryogenically cooled to maintain the detector temperature at 147 K to minimize the dark current. The 1 liter dewar allows for 24 hours of cryogen autonomy.

5.7 CCD Camera

The beam profile must be measured during the experiment. The beam profile is captured with a 16 bit Deep Sky Imager (DSI), sold by Meade Instruments Corporation. It features the Sony Super Hole Accumulation Diode (HAD) silicon CCD sensor. The detector has a sensitive region of 5 mm by 3.7 mm and a total of 250 000 pixels.

5.8 The Heating Chamber Assembly

During one portion of the experiment the temperature of the sample needs to be raised up to 350°C. To prevent oxidation and to thermally isolate the sample it is mounted in an evacuated heating chamber. The chamber is a stainless steel Ultra High Vacuum Cross sold by MDG MFG Inc, adapted with four Conflat flange access ports. Pictures of the chamber are shown in Figure 5.5 and Figure 5.6.

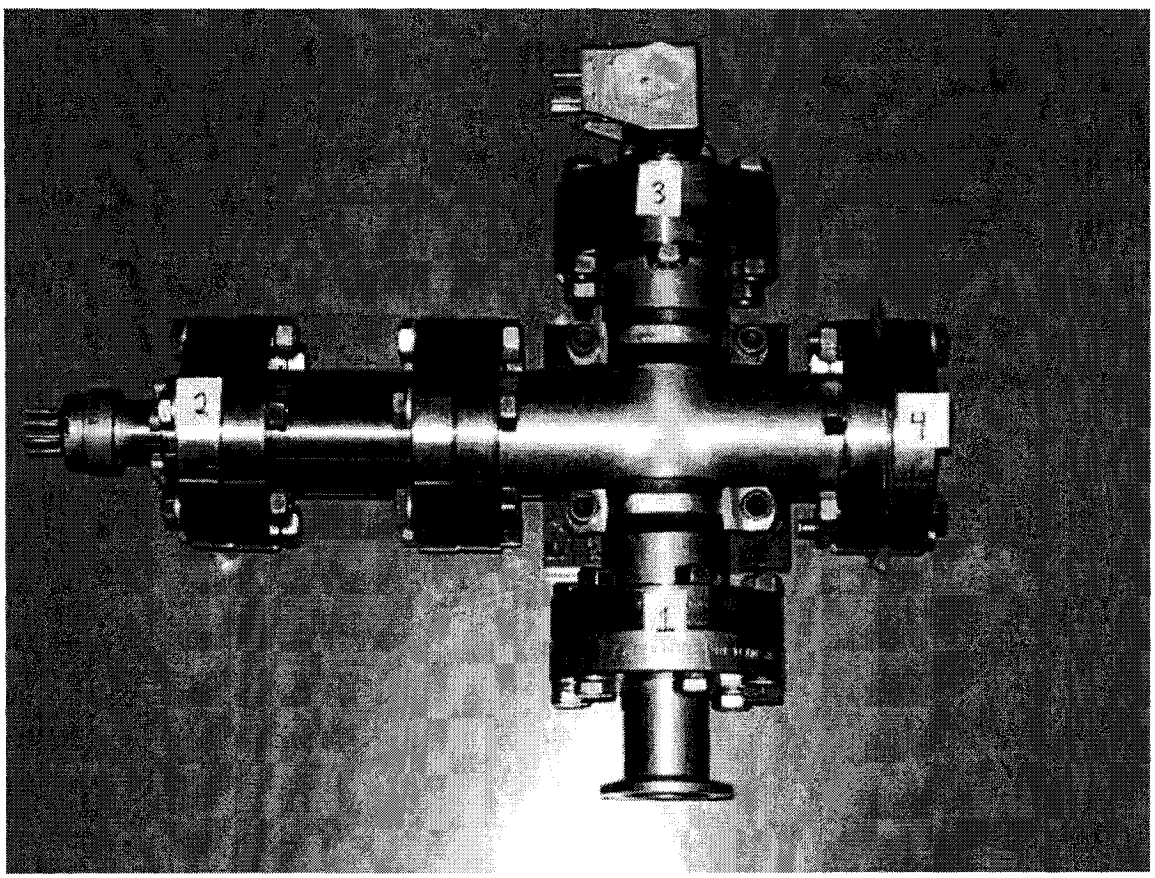

Figure 5.5 : Overhead view of the vacuum chamber showing its four ports. The bottom port (1) is the vacuum port, the left port (2) is the electrical feed though for the heater, the top port (3) is the electrical feed through for the thermocouple, and the right port (4) holds the copper heating head and is where the sample lies.

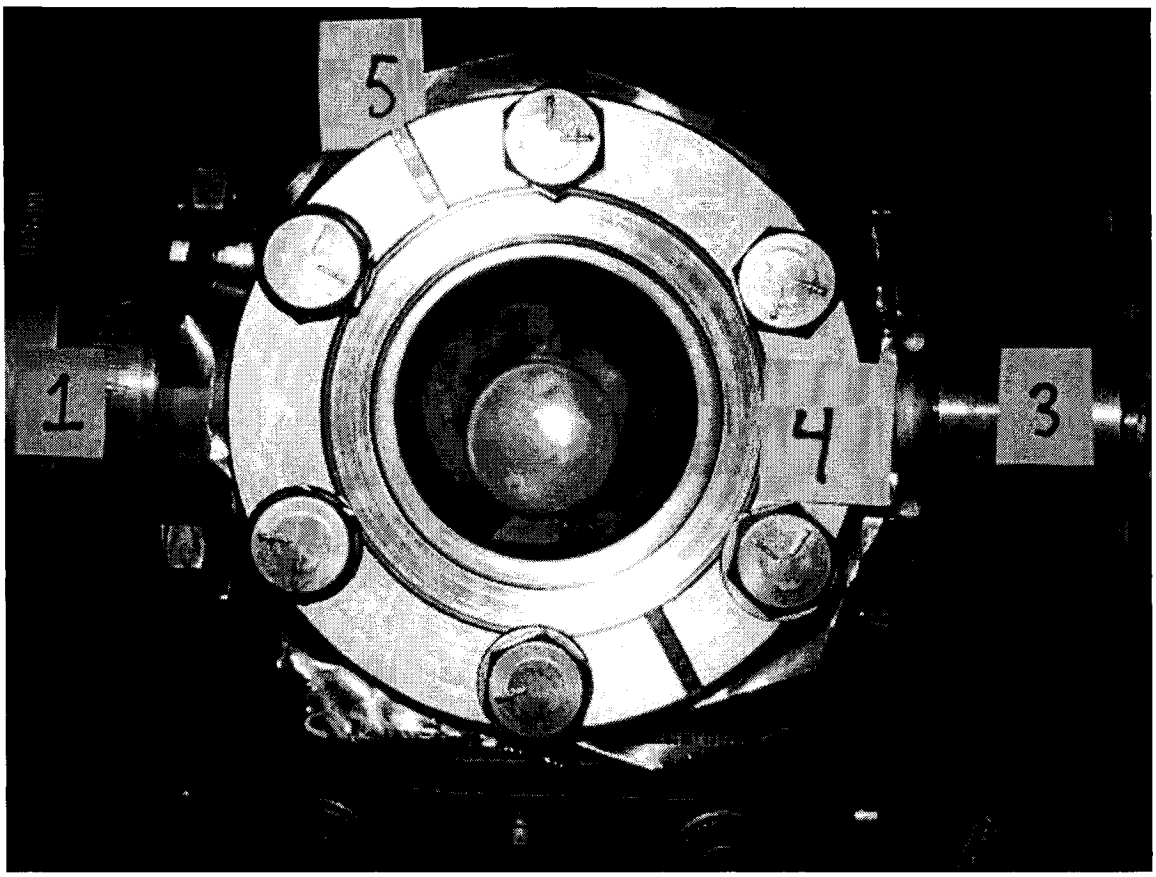

Figure 5.6 : Front view of the chamber. The vacuum port (1) and thermocouple feed through port (3) are shown. The front port (4) has the brown copper heating head at its center, and is covered by the Mylar window (5).

Inside the chamber, accurate temperature monitoring and control is needed. The sample is mounted on a copper heating head inside the chamber and affixed with Z9 Silicone heat sink compound. Z9 is a compound of zinc oxide and grease sold by GC Chemicals.[30] A small hole is drilled at the side of the copper head and a thermocouple is secured within with thermal conductivity paste. The thermocouple used is a K type bare thermocouple sold by Omega Engineering Inc.[31] It has a wire diameter of 3.8 mm and a maximum service temperature of 900°C. This arrangement assures that the sample is at the same temperature as the thermocouple and its temperature is accurately measured.

In the heating chamber, a high vacuum of 10^{-6} Torr is desired to ensure that the samples do not oxidize and the temperature remains stable. This requires the use of two vacuum pumps. The first pump is the mechanical pump, also known as a roughing pump. The useable range of this pump is between atmospheric pressure and 10^{-3} Torr. The second pump is a turbo pump which can only be initiated with pressures below 10^{-3} Torr, and has a useful range of 10^{-6} Torr. The pressure sensor used is an IKR 020 Cold Cathode gauge sold by Balzers-Pfeiffer.

The desired pressure of 1×10^{-6} Torr is not achieved without heating as a temperature of 50°C aids in offgassing in the chamber. Generally the vacuum of 10^{-4} Torr is achieved in 10 minutes, and then the temperature is raised and maintained at 50°C. After 30 minutes the heating is turned off and the chamber returned to room temperature. This procedure allows the vacuum to reach 1×10^{-6} Torr in approximately 60 minutes.

Once a good vacuum is established, resistive heating of the copper head begins. The heating head is a high temperature cartridge heater sold by McMaster-Carr. It is 2.54 cm in length and 0.63 cm in diameter, coated in bonded graphite and surrounded by an Incoloy sheath.[32] The heating head is mounted in a copper mount in the chamber and has a maximum operating temperature of 1150 K. The heater operated at 120 VAC and has a maximum allowable current of 0.66 Amps. The maximum amount of heating power delivered by the heater is 80 W. With this setup the temperature in the chamber under vacuum increased from ambient temperatures by about 100 K in 20 seconds. Depending on the pressure of the chamber, the temperature can drop 100 K in about one hour. The pressure inside the chamber is not constant during heating. As the chamber is heated to 300°C, offgassing causes the pressure to normally increase to 1×10^{-4} Torr.

5.9 Heating Chamber Temperature Control

The temperature inside the chamber is controlled with a proportional-integral-derivative controller (PID), the ISeries i16 Temperature and Process Controller sold by Omega Engineering. It is useable up to temperatures of 1400°C, and when combined with a K thermocouple has an absolute instrumental precision of 0.4°C in that range.[33] It is an active controller, and has an automated tuning function.

After a certain temperature is reached, several minutes are needed before the temperature stabilizes. The lower temperatures require more time to stabilize than the higher temperatures. This is because the higher temperatures induce higher heat losses, and when the temperature overshoots they return to the desired set point faster. It is common for temperatures below 100°C to overshoot by 20°C and to require 10 minutes to lower to the desired temperature, and then repeat the cycle. A temperature near 300°C would only overshoot by 2°C, fall to the desired temperature and maintain that temperature indefinitely.

As shown in Figure 5.5 and Figure 5.6, the vacuum chamber has four ports. One of the ports is attached to the vacuum pumps and two others are used for electrical wiring. The sample is placed in front of the final remaining port. Over that port is placed a piece of 23 μm thick Mylar 800. Mylar 800 is a polymer base film made by Dupont that can sustain high temperatures and stress without tearing.[34] The Mylar sheet is secured with a flange. Six holes are burned in the Mylar with a soldering iron which allow screws to be used to fasten the covering in place. Between the Mylar and the vacuum chamber an O-ring gasket is used which is lubricated with vacuum grease.

Mylar is used primarily because of its flexibility. When the chamber is evacuated, a pressure difference acts on the film and causes it to deform inward. This creates a concave surface which allows the objective of the microscope to be placed closer to the sample than if a solid glass window were used. This allows for a high magnification objective to be used resulting in more of the scattered signal being collected. Anytime that heat to the chamber is activated there is a risk of damaging the microscope objectives, and air is blown across the gap between the microscope lens and the vacuum chamber to cool the objectives to prevent any thermal damage.

The vacuum chamber is then mounted on an XYZ stage in front of the microscope objective. The microscope objective is a Mitutoyo M PLAN APO 20X, NA 0.40 with a working distance of 20.0 mm. The microscope remains fixed, and the relative position of the chamber is adjusted until the sample is at the focal point of the microscope. A moveable mirror is positioned into the optical path of the microscope so that some of the scattered light is sent to a video camera, which aids in the alignment. This is shown in Figure 5.1.

5.10 Laser Heating of the Sample

Laser heating can cause large temperature increases at the laser spot. Gallium sulfide is stable in air and no special precautions are necessary for simple laser heating. Silicon oxidizes at high temperatures in air and it is laser heated in a vacuum even at room temperature. In air, gallium sulfide is mounted on a glass slide with either double sided tape or vacuum grease depending on its size. The low thermal conductivity of glass minimizes heat transfer away from the sample. In the vacuum chamber silicon is mounted

directly onto the copper heating head. The glass slide or the vacuum chamber are placed on an XYZ stage and moved to the focal point of the microscope.

5.11 Sample Choice

Two sample materials are used in the experiment. Silicon is chosen as a test material because it is widely available, relatively inexpensive, and has been very highly characterized. GaS is chosen because its properties are superior to silicon's for our purposes. At room temperature GaS has a thermal conductivity of 10 W/m K in one direction and 105 W/m K in a second,[35] which is lower than that of silicon of 150 W/mK.[2] GaS also has a much stronger Raman signal, and a nearly identical Raman shift dependence on temperature as silicon. There are also no phase transitions for either material through the experimental temperature range. The dimensions of the silicon sample used are 5 mm by 7 mm, and of the gallium sulfide sample are 2 mm by 3 mm.

The complicating factor with GaS is that it has a layered structure.[39] In the direction parallel to the layers, the material is held together with strong covalent bonds. In the direction perpendicular to the sheets, the sheets are attached to other sheets through weak van der Waals forces. This results in strong interatomic forces parallel to the sheets and a subsequent high thermal conductivity of 105 W/ m K, and weak interatomic forces between sheets and a low thermal conductivity of 10 W / m K. This directionally dependent thermal conductivity affects the results obtained during the experiment.

Chapter 6: Experimental Procedure

6.1 Introduction

Before experiments are performed, the entire optical system must be aligned and calibrated. The experiment performed consists of two main parts. The first is determining the Raman shift's temperature dependence. The second is heating the sample with incident laser light to induce a temperature increase. The results of these two experiments are combined to calculate the thermal conductivity of the sample.

6.2 Laser Spot Diameter

The first measurement that must be made is the diameter of the beam spot. Once the optical experimental setup is optimized, the chamber is removed, and the Meade Deep Sky Imager (DSI) is placed at the location of the sample. The DSI is a CCD camera, and a profile of the laser beam waist is taken. Optical density filters are placed in front of the laser, reducing the laser intensity to ensure that saturation of the camera does not occur. To increase the dynamic range of the instrument, several hundred exposures are taken and averaged together. This gives an intensity profile of the beam spot. This profile is fitted with a Gaussian curve, and its diameter is measured in the number of pixels it covers on the camera.

The camera field of view, given the optical configuration, is then calibrated. The silicon sample is moved so that an edge is visible when viewed on the DSI. The edge is moved to the bottom of the screen. The stage is motorized and moved by a precise distance until the sample's edge is at the very top of the screen. The distance moved, as

measured by the motor encoder, is the vertical scale of the DSI. The CCD field of view is vertically 492 pixels long, and therefore a calibration of vertical pixels to μm is made. This process is repeated in the horizontal direction.

6.3 Standardized Measurement

Before carrying out experiments, the Raman spectrum of silicon is taken for a standardized time and incident laser power. Generally a laser output power of 200 mW is used, which correlates to roughly 100 mW on the sample. The signal is integrated for 10 s for weak Raman scatterers such as silicon, and approximately 1 s for stronger Raman scatterers. This process ensures that the positioning of the sample is correct. A standardized measurement of a spectrum of silicon outside of the vacuum chamber is taken each day to compare the quality of the alignments from day to day.

Several Raman spectra are then recorded with various exposure times to determine how long an exposure can be before the detector is saturated. This gives an important baseline for the subsequent exposure at higher temperatures. As the temperature is raised, signal broadening occurs, and thus peak intensity decreases. To achieve similar statistical uncertainties for the peak position of the Raman shift at different temperatures, the integration time of higher temperature exposures must be increased.

6.4 Measuring the Raman Shift's Temperature Dependence

The first part of the experiment is determining the Raman shift's temperature dependence of the sample. Quantifying this Raman shift allows the temperature change in

a material to be determined. The purpose of the first portion of the experiment is to calibrate the Raman signal into an optical thermometer.

With the sample affixed in the evacuated vacuum chamber, a Raman spectrum is collected at 50° C intervals as the temperature is increased systematically from room temperature to 350°C. As all that is required is relative changes in the Raman shift with temperature, no frequency calibration was done during the experiment. Three Raman spectra are collected at every temperature. The spectra are converted to ASCII format, and viewed and curve-fitted using XRDA.[36] The resulting spectra are analyzed to determine the Raman shift at various temperatures. A linear regression is then performed to determine the slope, which is the change in the Raman shift in cm^{-1} per Kelvin.

The heating effect of the laser beam on the sample is relatively small as low power was used, and does not affect the temperature of the sample. In comparison to the resistive heating supplied by the copper heating head, only a small amount of energy is supplied to the sample by the laser, and the temperature measured by the thermocouple does not change with a change in laser power. Raman spectra were taken at several different laser powers at each elevated temperature, and no difference in their Raman shifts was found. This is shown in Figure 6.1.

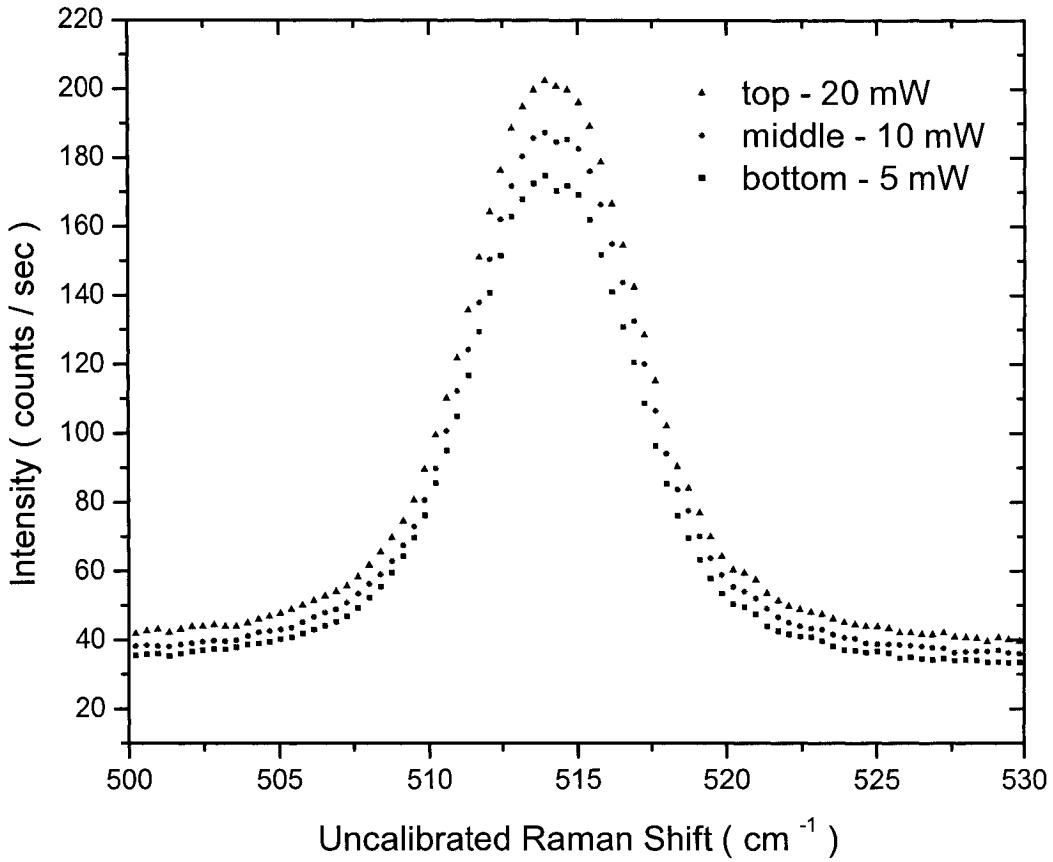

Figure 6.1 : Raman shift induced by laser heating silicon at low laser power. The bulk sample temperature of the silicon is maintained at 100° C. The top spectrum line is achieved at 20 mW, the middle spectrum with 10 mW, and the bottom with 5 mW. The data sets are normalized to have comparable maximum heights, yet to also not overlap and remain distinguishable. The Raman shift was not calibrated as only relative shifts of the Raman position are important for the experiment.

6.5 Determining the Temperature Shift Caused by Laser Heating

The second portion of the experiment is to use a focused laser beam to induce a temperature rise on the surface of a sample. This temperature rise is detected using the shift in the Raman spectrum, as described earlier. By measuring the change in temperature at the surface, the size of the laser spot, and the amount of absorbed laser power, the thermal conductivity of the sample is calculated using the Equation 4.30.

The laser heating begins with low laser power, generally 20 mW. The sample comes to thermal equilibrium, and generally three Raman spectra are collected at that particular laser power. The power is increased and the sample settles for several minutes, then another sequence of Raman spectra is collected. Once again, as only relative changes are necessary, the wavelength of the Raman light is not calibrated to determine its absolute wavelength. The Raman shifts for several incident powers are measured. A linear regression is performed on the data of Raman shift versus incident power, with the slope being the dependence of the Raman shift on incident power.

Chapter 7 : Results

7.1 Introduction

The all optical thermal conductivity experiment produces two main results. The first is the measurement of the Raman signal's temperature dependence for both silicon and gallium sulfide. The second is the measurement of the thermal conductivity of silicon at three different temperatures and gallium sulfide at room temperature. Completing the measurements requires measuring the intensity of the laser at the sample, imaging and curve fitting the beam profile, measuring and curve fitting the Raman lines as a function of laser power at different temperatures, and finally calculating the thermal conductivity according to Equations 4.30. The results are found to agree with published values for silicon, but are always biased toward the upper end of the acceptable values. The temperature rise in the silicon samples shows nonlinearity at higher temperatures. The thermal conductivity for GaS is found to be outside the range of published values.

7.2 Raman Spectra of Silicon and Gallium Sulfide

The Raman spectra of silicon and gallium sulfide are shown in Figures 7.1 and 7.2, respectively. The collected Raman lines are fitted with a Lorenztian line profile with a linear baseline using the XRDA software. The center of the peak, the area, and the FWHM are extracted from the fit.

A Lorenztian line shape is appropriate here because the interactions of light with matter are semi-classically modeled as a forced harmonic oscillator under the influence of a frictional term. This forced oscillation causes the accelerated electron to radiate

electromagnetic radiation, which decays the oscillation in an exponential fashion. Anytime that one has a decaying exponential signal in the time domain, a Lorenztian line shape in the frequency domain is obtained.[37] The details of these processes are beyond the scope of this thesis.

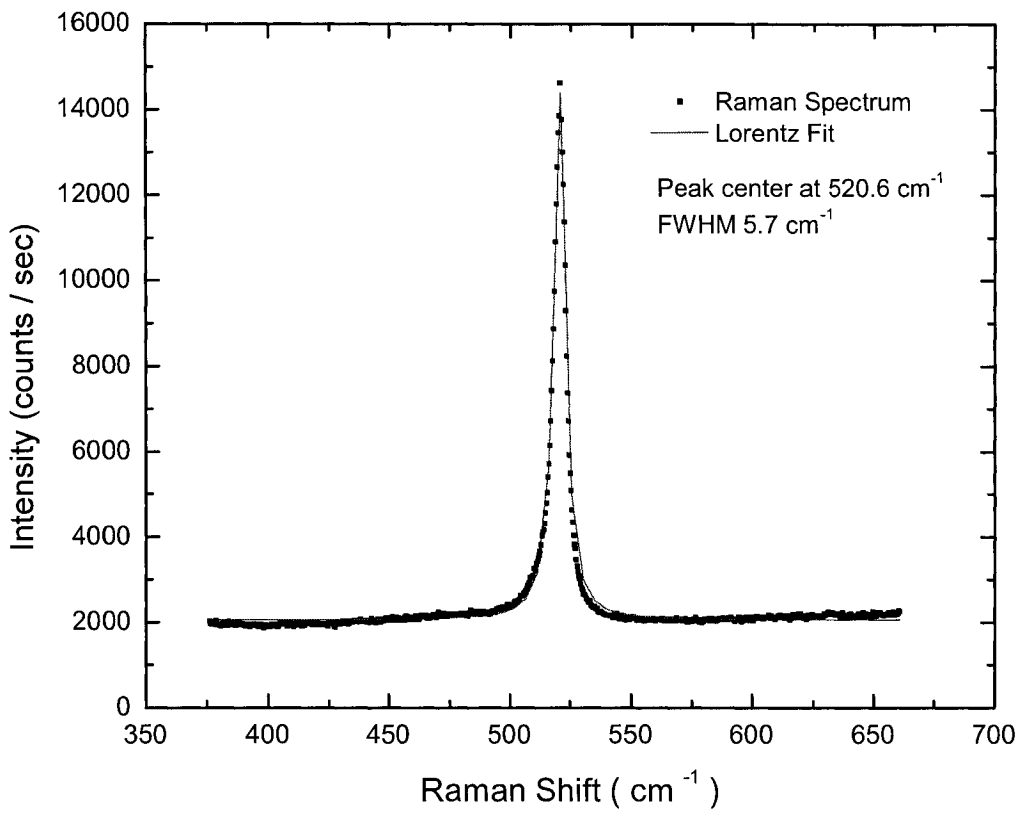

Figure 7.1 : Stokes Raman spectrum of silicon (symbols), fitted with a Lorenztian line profile (solid line). The fitting is done with XRDA. The silicon is at 23 °C under vacuum with 215 mW of incident laser power. The Raman shift is not calibrated as only relative shifts of the Raman position are important for the experiment. The peak center is at 520.6 cm^{-1}, with a FWHM of 5.7 cm^{-1}.

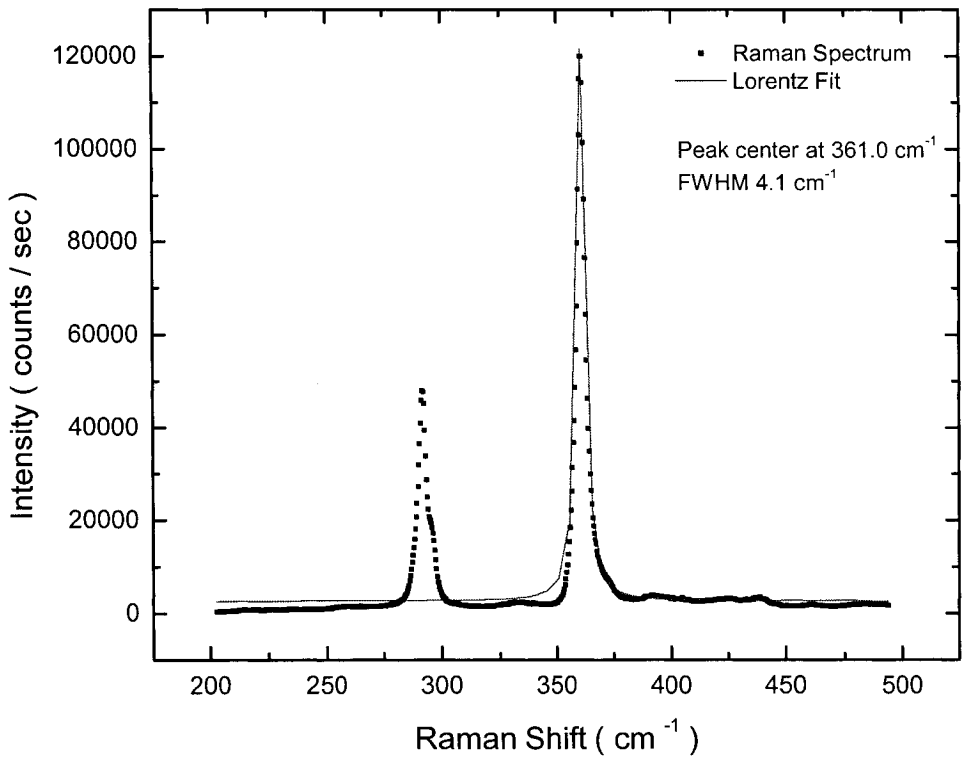

Figure 7.2 : Stokes Raman spectrum of gallium sulfide (symbols), fitted with a Lorenztian line profile (solid line). The fitting is done with XRDA. The gallium sulfide is at 23 °C in air with 140 mW of incident laser power. The Raman shift is not calibrated as only relative shifts of the Raman position are important for the experiment. The peak center is at 361.0 cm^{-1}, with a FWHM of 4.1 cm^{-1}. The peak centered near 290 cm^{-1} is not used in the experiment and is never fitted.

Two peaks are observed in the Raman spectrum of gallium sulfide. The first is near 290 cm^{-1} and the second is near 360 cm^{-1} . The 360 cm $^{-1}$ line is used in this experiment. As shown in Figure 7.2, the 360 cm^{-1} line is 2.5 times more intense than the 290 cm^{-1} line. Preliminary results also showed that the second Raman line of GaS had nearly twice the temperature dependence as the first line. These reasons made it clear that the 360 cm^{-1} would be much more useful as a temperature probe for gallium sulfide.

The line shape of silicon is much closer to an ideal Lorenztian than that for gallium sulfide. $\chi 2$-minimization is a statistical technique which describes the goodness

of fit of a theoretical line to a real set of data. The closer the reduced $\chi 2$ it is to 1, the better the fit of the experimental data. The reduced χ^2 for the silicon fit is 0.99, while for the 360 cm^{-1} line of gallium sulfide the reduced χ^2 value is 0.97. This is caused by the leading edge of the gallium sulfide's Raman spectrum. Although the silicon has a better line shape, the intensity of the GaS Raman signal leads to a smaller uncertainty in the peak position and more repeatable results. The uncertainty in the silicon peak position in Figure 7.1 is 0.05 cm^{-1} and for GaS in Figure 7.2 is 0.004 cm^{-1}.

7.3 Temperature Dependence of the Raman Shift

The first experimental result is the change in the Raman signal measured as a function of temperature. The result for silicon is shown in Figure 7.3. In accordance with the paper by Périchon *et al.* the Raman shift's temperature dependence was assumed to be linear, and is found to be -0.024 ± 0.002 cm^{-1} per K. This is within uncertainty of the value of -0.025 cm^{-1}/K published by Périchon *et al.*[2]

The experimental results of GaS show a comparable change in the Raman signal with temperature. The results are shown in Figure 7.4. The Raman signal dependence on temperature is -0.026 ± 0.001 cm^{-1} per K. This is slightly larger than the silicon shift. No published results for the temperature dependence of gallium sulfide's Raman shift were found. The uncertainty in the temperature dependence of GaS is smaller than for Si. The Raman signal of GaS has a larger signal-to-noise ratio than Si. The uncertainty in the peak position is found by measuring the Raman spectrum three times for each temperature and taking the spread in the data as the uncertainty in the measurement. Although the silicon spectrum was better fitted by a Lorenztian line profile, the stronger

Raman signal of GaS results in a better defined central peak position, and therefore a smaller spread in the data collected. This leads to a smaller uncertainty in the peak position of the Raman shifts for each temperature, and thus for the slope of the linear regression.

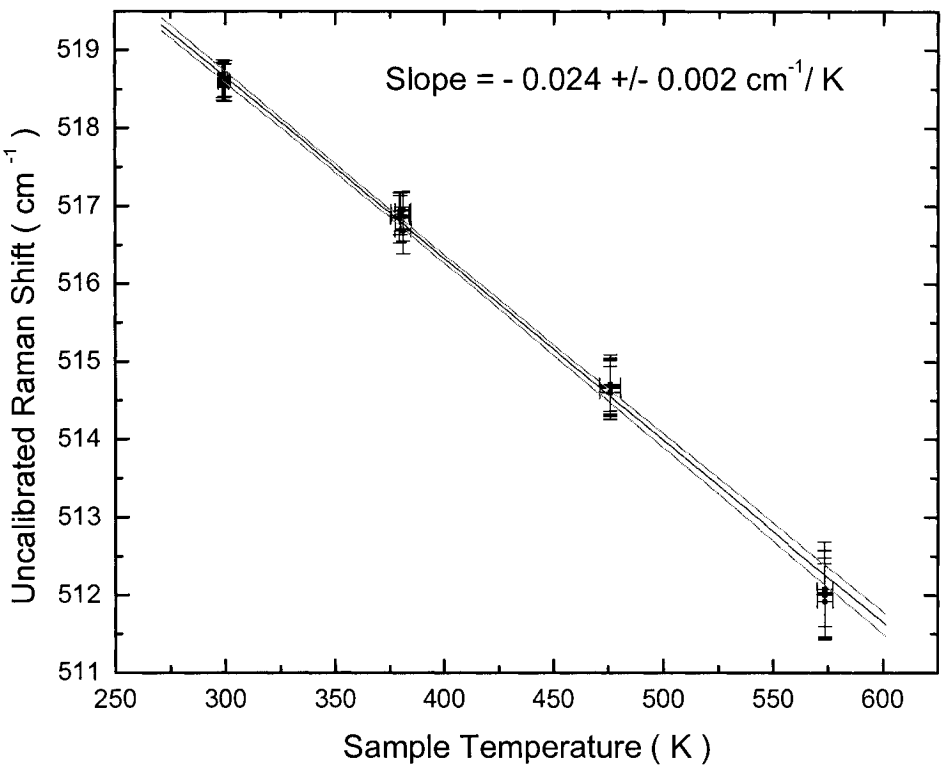

Figure 7.3 : Measured Raman shift of silicon due to resistive heating inside of a vacuum chamber. In the linear regression the data is weighed according to the uncertainty bars shown. The incident laser power is 100 mW of 488 nm wavelength unpolarized light. No laser induced heating is seen as discussed in Chapter 6. The dependence is -0.024 $\pm$ 0.002 cm^{-1} per K. Since only the relative changes in shift are important for our purposes, no calibration is done to determine absolute Raman shifts. The dashed lines represent the 95 % confidence interval.

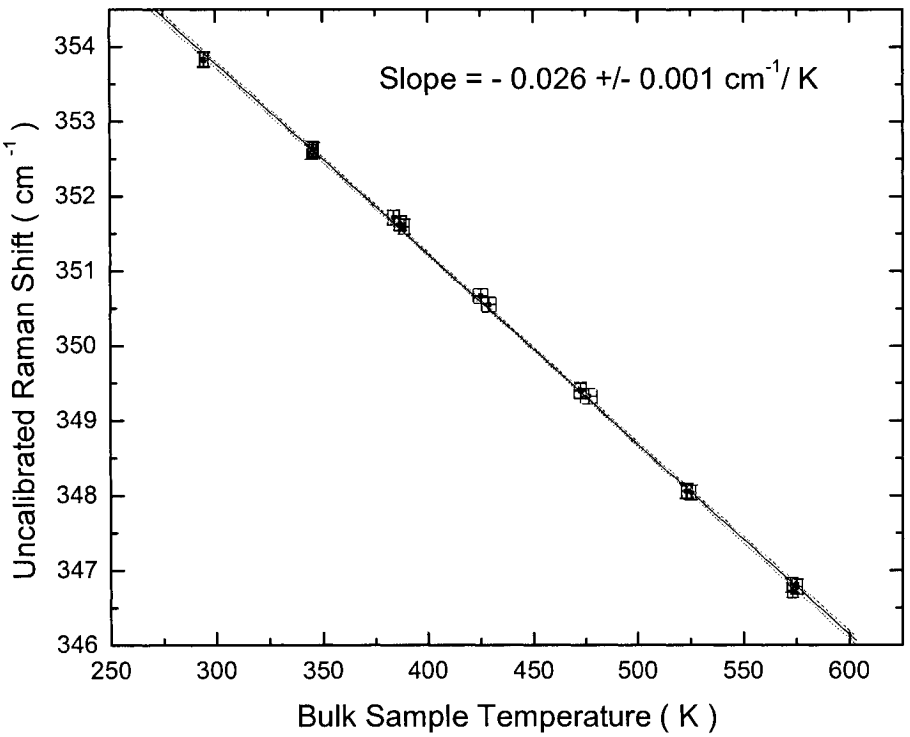

Figure 7.4 : Measured Raman shift of gallium sulfide due to resistive heating inside of a vacuum chamber. Uncertainty bars are shown on graph, but too small to be visible. In the linear regression the data is weighed according to the uncertainty bars shown. The incident laser power is 100 mW of 488 nm wavelength unpolarized light. No laser induced heating is seen as discussed in Chapter 6. The dependence is -0.026 $\pm$ 0.001 cm^{-1} per K. Since all that is important is the relative change in the Raman shift, no calibration is done to determine absolute Raman shifts. The dashed lines represent the 95 % confidence interval.

The Raman shift's temperature dependence for gallium sulfide and silicon are measured. The measured temperature dependence now allows the use of the Raman scattering process as a temperature probe for a thermal conductivity measurement. The all optical thermometer is now established.

7.4 Measured Thermal Conductivity

The second experimental result is the shift in a material's Raman signal resulting from heating by a known amount of incident laser power. Before this is calculated, the laser spot size is measured using a 16 bit CCD camera, the Meade Deep Ski Imager. An intensity profile of the beam is taken and the camera's pixel size is calibrated. In the vertical direction the camera has 492 pixels and, given the optical configuration, has a field of view of 270 +/- 10 μm. Assuming similar results in the horizontal direction, each pixel measures 0.55 +/- 0.02 μm. The beam spot is imaged and its intensity is shown in Figure 7.5.

The criteria for the beam spot width used by Cline *et al.* for the derivation of Equation 4.30 is the width at which the beam reduced to $1/e^2$ of its peak intensity. This definition is used to simplify the mathematics of the derivation. Using this criterion, cross sections of the beam were chosen and Origin[38] fitted each beam profile. Various cross sections of different orientations were chosen and their fits compared. The beam spot was found to be approximately circular with a beam diameter averaging 28 pixels +/- 4 pixels. That equates to a circular beam spot waist of 16 +/- 2 μm.

The incident laser light caused a shift in the Raman signal of the various materials. Spectra of silicon at different incident powers are shown in Figure 7.6. The difference between the spectra of silicon absorbing 33 mW of laser power and 189 mW of laser power is shown and the shift in the Raman peak position is readily visible.

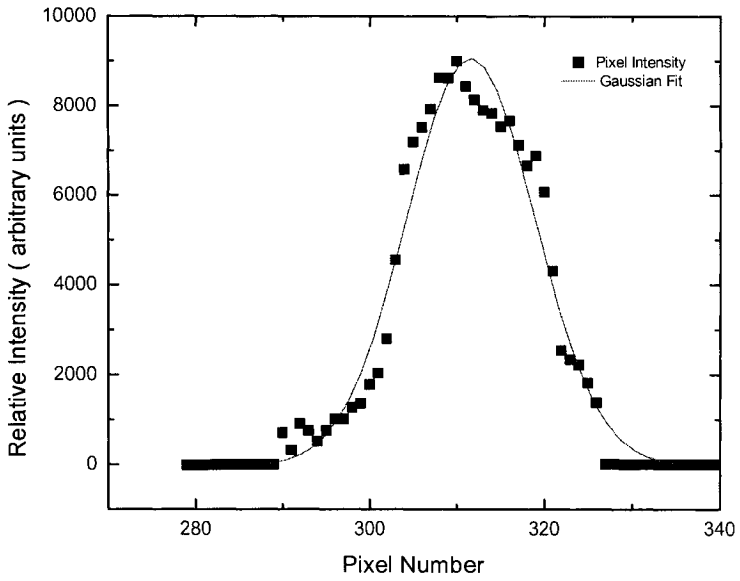

Figure 7.5 : Beam Intensity profile taken with a Meade Deep Sky Imager 16-bit CCD camera. The pixel intensities (symbols) are fitted with a Gaussian line profile (solid line) with a linear background.

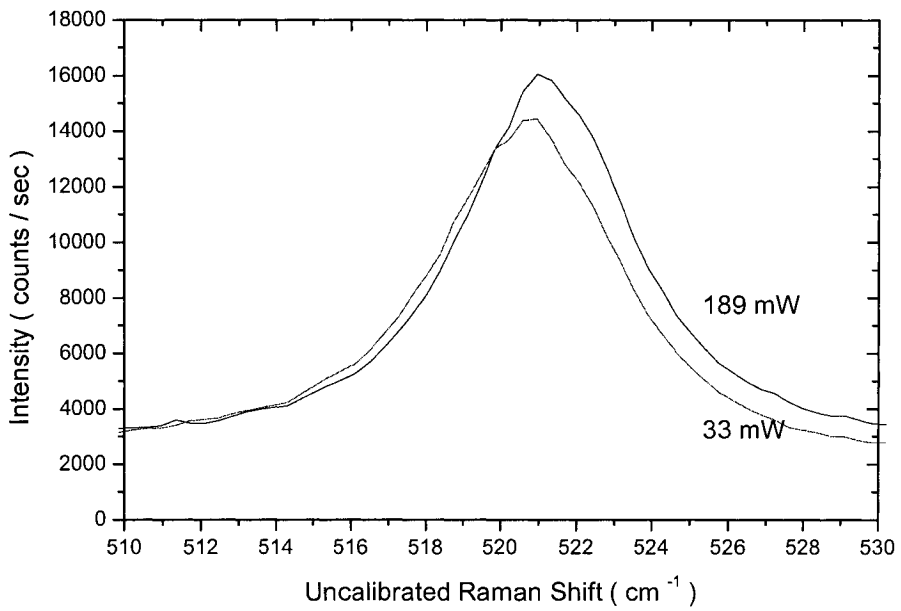

Figure 7.6 : Raman shift induced by laser heating silicon at high laser power. The bulk sample temperature of the silicon is 23° C. The two spectra are labeled, with the bottom most spectrum achieved with 33 mW of absorbed laser power by the sample, and the top spectra achieved with 189 mW of absorbed laser power by the sample. The data sets are normalized to have comparable maximum heights. The Raman shift is not calibrated as only relative shifts of the Raman position are important for the experiment. The total shift in the peak position is 0.7 cm^{-1}.

The result for the laser heating of silicon at 23 +/- 1 °C is plotted in Figure 7.7.

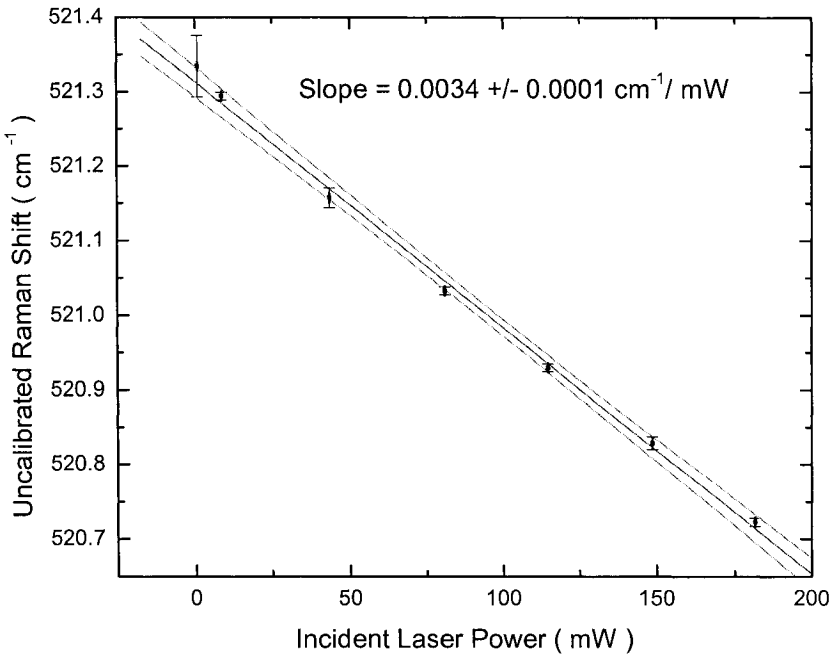

Figure 7.7: Measured Raman shift of silicon resulting from an increase of surface temperature due to laser light heating. The silicon sample is at 23 ± 1 °C and the incident laser light wavelength used is 532 nm. The linear regression is done in Origin, with the data pointed weighted by their uncertainty. Uncertainty bars are shown in both x and y for all data points but are too small to see. The slope of the graph is 0.0034 ± 0.0001 cm^{-1}per mW. Since all that is important is the relative change in the Raman shift, no calibration is done to determine absolute Raman shifts. The dashed lines represent the 95 % confidence interval.

For silicon S_{Temp} is 0.024 ± 0.002 cm^{-1} per K, S_{Heat} of silicon at 23 ± 1 °C is 0.0034 ± 0.0001 cm^{-1} per mW, and the reflectivity at 532 nm is 37.4 %.[20] By Equation 4.30 and with a measured spot size of 16 ± 2 μm, the thermal conductivity of silicon is found to be 175 ± 31 W/m K. This is within uncertainty of the published value of 150 W/m K, at room temperature.[20]

The results of Périchon *et al.* are different than those obtained in the present work. They found that the thermal conductivity of porous silicon was 63 ± 10 W/mK with a bulk temperature of 500 °C.[2] It is not very useful to compare that value with the results

obtained here because Périchon *et al.*'s results were on porous silicon. The exact amount and spacing of air pockets in porous silicon greatly alter the thermal conductivity. In the same paper other published values for porous silicon are mentioned as 35 W/mK and 45 W/mK. [2] One useful comparison is that the relative uncertainty in Périchon et al.'s data is 16%, which it comparable to the uncertainty in this experiment of 18% for the thermal conductivity.

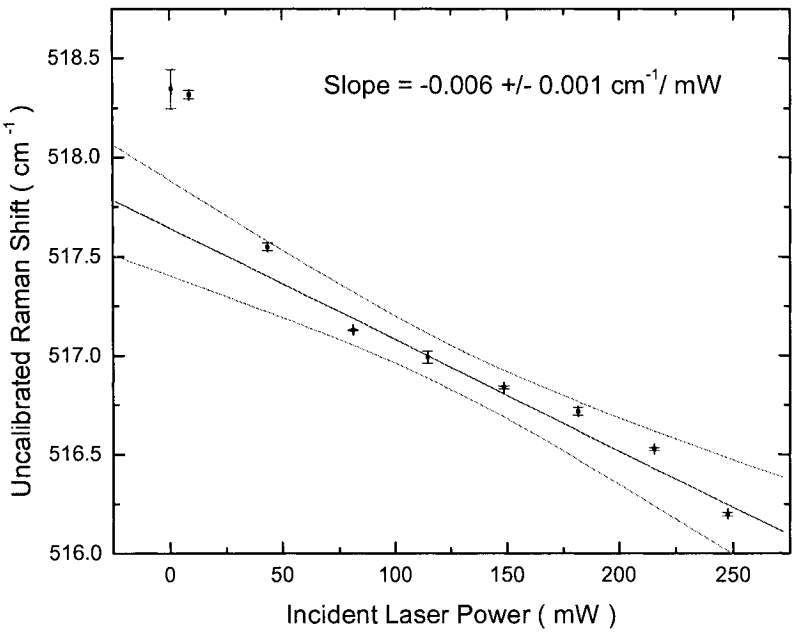

Figure 7.8: Measured Raman shift of silicon resulting from an increase of surface temperature due to laser light heating. The silicon sample is at 200.0 ± 0.1 °C and the incident laser light wavelength used is 532 nm. The linear regression was done in Origin, with the data pointed weighted by their uncertainty. Uncertainty bars are shown in both x and y for all data points but are too small to see. The slope of the graph is 0.006 ± 0.001 cm^{-1}per mW. Since all that is important is the relative change in the Raman shift, no calibration is done to determine absolute Raman shifts. The dashed lines represent the 95 % confidence interval.

The silicon bulk sample temperature is increased to 200 °C and laser heated. This is shown in Figure 7.8. Data points at higher laser powers were not included in the fit, as will be discussed in Section 8.1. S_{Heat} for silicon at 200.0 °C ± 0.1 is 0.006 ± 0.001 cm^{-1}

per mW. By Equation 4.30, and with a reflectivity at 200 °C of 38.7 %,[20] the thermal conductivity is found to be 104 ± 24 W/m K. This is within uncertainty of the published value of 80 W/m K.[20]

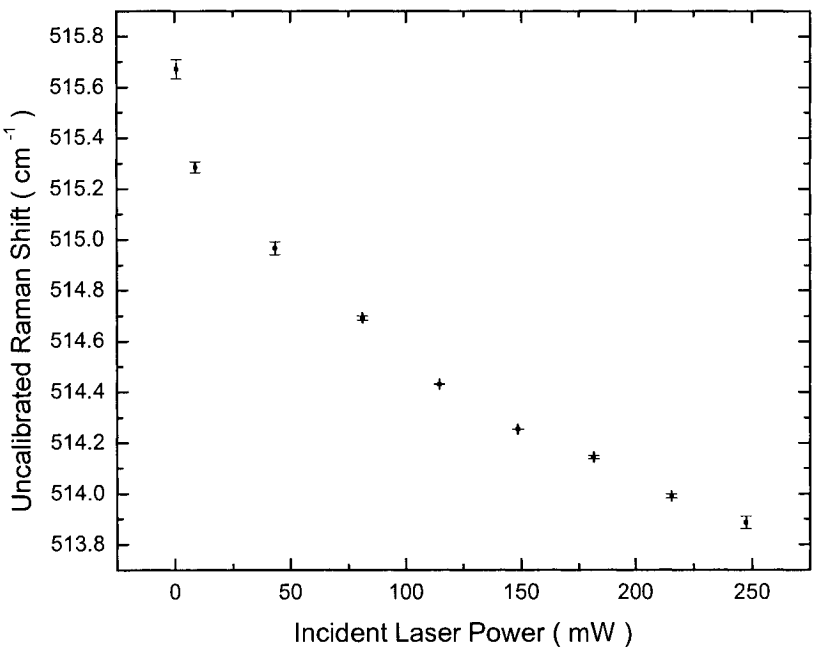

Figure 7.9: Measured Raman shift of silicon resulting from an increase of surface temperature due to laser light heating. The silicon sample is at 300.0 ± 0.1 °C and the incident laser light wavelength used is 532 nm. Uncertainty bars are plotted in both x and y for all data points but are too small to see.

The laser heating of silicon with a bulk temperature of 300 °C is shown in Figure 7.9. The data for silicon at 300 °C was difficult to analyze. The dependence of the Raman shift with incident laser power is not linear, and this feature is discussed in Section 8.1. The middle part of the graph, which is approximately linear, is used in the analyses and shown in Figure 7.10.

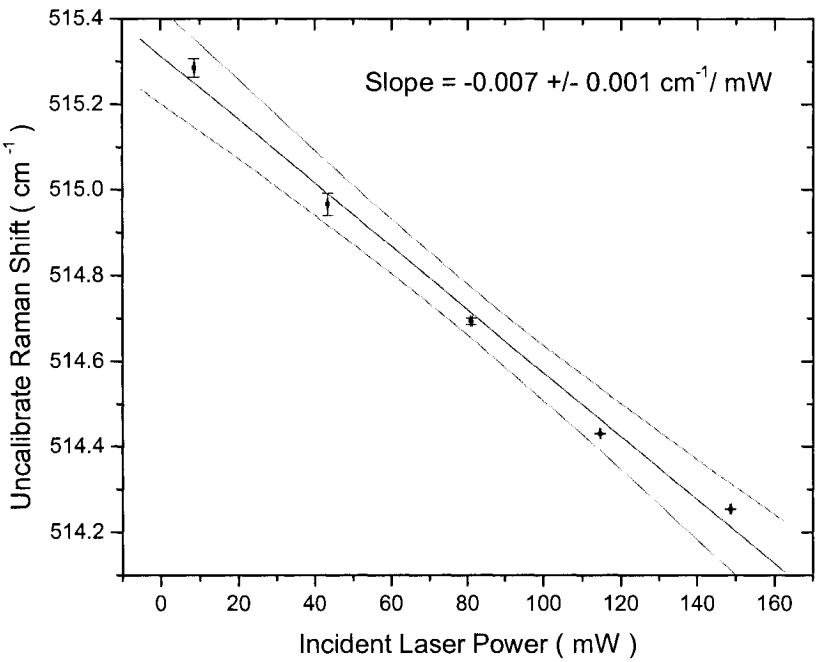

Figure 7.10: Measured Raman shift of silicon resulting from an increase of surface temperature due to laser light heating. The silicon sample is at 300 °C and the incident laser light wavelength used is 532 nm. Only the middle values of incident power are used. The linear regression is done in Origin, with the data pointed weighted by their uncertainty. Uncertainty bars are plotted in both x and y for all data points but are too small to see. The slope of the graph is 0.007 ± 0.001 cm^{-1}per mW. Since all that is important is the relative change in the Raman shift, no calibration is done to determine absolute Raman shifts. The dashed lines represent the 95 % confidence interval.

As shown in Figure 7.10, at 300.0 ± 0.1 °C , S_{Heat} for silicon is 0.007 +/- 0.001 cm^{-1} per mW. By Equation 4.30, and with a reflectivity at 300 °C of 39.2 %,[20] the thermal conductivity is found to be 79 ± 18 W/m K. This is within uncertainty of the published value of 63 W/m K.[20]

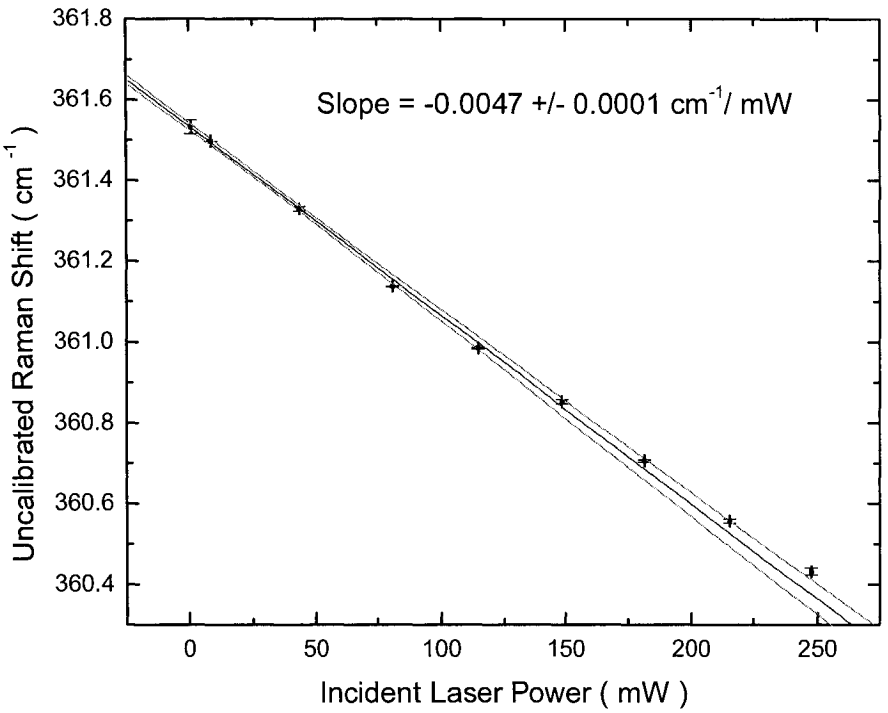

Figure 7.11 : Measured Raman shift of gallium sulfide resulting from an increase of surface temperature due to laser light heating. The sample is at 23 +/- 1 °C and the incident laser light wavelength used is 532 nm. The linear regression is done in Origin, with the data pointed weighted by uncertainty in the regression. Uncertainty bars are plotted in both x and y for all data points but are too small to see. The slope of the graph is 0.0047 ± 0.0001 cm^{-1} per mW. Since all that is important is the relative change in the Raman shift, no calibration is done to determine absolute Raman shifts. The dashed lines represent the 95 % confidence interval.

The shift in the Raman signal for gallium sulfide is shown in Figure 7.11. The S_{Temp} is 0.026 +/- 0.001 cm^{-1} per K, S_{Heat} = 0.0047 +/- 0.0001 cm^{-1} per mW, the reflectivity at 532 nm is 52 %.[39] Utilizing a beam spot size of 16 +/- 2 μm and Equation 4.30, the thermal conductivity of GaS at 23 +/- 1 °C is 87 +/- 12 W/m K. The previous published values are 105 W/m K for perpendicular to the beam, and 10 W/m K parallel to the beam.[36] This discrepancy is discussed in Section 8.1.

Chapter 8 : Discussion

8.1 Introduction

The Raman shift's temperature dependence is found to agree well with published values for silicon and GaS. Reasons for the thermal conductivity of silicon being consistently high and showing nonlinearity are discussed. Possible reasons are heat diffusing away from the laser spot, thermal contact with the copper heating head of the heating chamber, the temperature dependence of the thermal conductivity and the reflectivity, thermally induced strain gradients and photoelastic effects. The thermal conductivity for GaS do not match with published results, and a possible reason for this relates to its layered structure. Improvements to the experiment are mentioned. As a first attempt, the all optical thermal conductivity experiment is found to have promise, and would be possible to extend to the diamond anvil cell.

8.2 Discussion of Results

The Raman shift's temperature dependence for silicon was investigated from 23 °C to 300 °C, and for gallium sulfide at 23 °C. This range was not extended further because the silicon peak became too broad after that temperature. The purpose of using gallium sulfide was that it was a stronger Raman scatterer, and it was meant to be used if silicon proved too difficult to measure. Once silicon was shown to have an adequate Raman signal, all available time and effort was spent on improving the silicon signal, and consequently no higher temperature gallium sulfide thermal conductivity measurements

were made. Gallium sulfide did serve the purpose of proving the usefulness of the measurement method to samples beyond silicon.

The Raman shift's temperature dependence for silicon agrees with published values. It also has the proper trend of decreasing Raman shift with increased temperature. This decrease makes sense, qualitatively. The Raman shift is a measure of the bond stiffness between adjacent atoms. As the temperature increases, thermal expansion of the material causes the bond stiffness to decrease. This leads to the decrease in the Raman shift with temperature measured in the experiment. This also agrees with theory as the temperature dependence of the thermal conductivity was modeled by an inverse temperature dependence by Moody *et al.*[20]

The changes in the Raman shifts for both GaS and silicon are adequately large to be useful, being 0.026 cm^{-1}/K and 0.024 cm^{-1}/K, respectively. The Raman peak position is usually measured within a precision of 0.02 cm^{-1} for the Raman spectra collected in this experiment. If the Raman shift is used as a thermometer, the temperature measurement would have a precision of 0.8 K for both GaS and silicon. In the all optical thermal conductivity method described, the smallest temperature rise was 31 K, and the largest source of experimental uncertainty was nearly always the laser beam diameter. For this experiment the Raman shift was a convenient, accurate temperature measurement.

The sample choices were also appropriate. The choice of silicon as a reference sample proved useful because its thermal conductivity is published at the different temperatures investigated in this thesis, 23 °C, 200 °C and 300 °C. The reflectivity of silicon is also readily available. Gallium sulfide was an excellent choice as a second

material. Its reflectivity at wavelengths from 400 nm to 800 nm and thermal conductivity at 23 °C are also published. Its Raman signal is much stronger which made for more accurate spectral measurements. As shown in Figure 7.1, the signal-to-noise ratio for that trial of silicon is 7.5 , which is typical for silicon in this experiment. As shown in Figure 7.2, the signal-to-noise ratio for that trial of GaS is 100, more than one order of magnitude greater than silicon. This leads to greater precision in the measured Raman shift's temperature dependence of GaS than that of silicon, with a relative uncertainty of 8.3 % for silicon and 3.8 % for GaS. This leads to a smaller uncertainty in the thermal conductivity measured, as relative uncertainty for the silicon trials ranged from 21 % – 24 %, while the uncertainty in the GaS measurement was 14 %.

The data collected for the Raman shift with incident laser light power for silicon at 300 °C and 200 °C are not linear. The non linearity did not occur for the silicon or gallium sulfide at room temperature. It also did not occur in the work of Périchon *et al.*[2] who found a linear relationship between absorbed laser power and the sample's temperature increase. The nonlinearity worsened as the temperature of the bulk sample increases and as the induced laser heating increases.

As the temperature of the bulk sample increases the thermal conductivity of the silicon decreases. As the incident laser power increases a greater temperature difference is established between the sample being heated by the laser and the surrounding bulk material. At 23 °C the silicon temperature rise at the beam spot was 14 K per 100 mW incident power, at 200 °C it was 24 K per 100 mW and at 300 °C the rise was 30 K per 100 mW. As the temperature gradient between the laser heated material and the bulk material increases, so does the heat transfer away from the heated area. This leads to a

perceived cooling effect on the laser heated region, which decreases the change in the Raman shift. This skews the linear Raman shift to laser power relationship into more of an exponential decay function at higher laser powers, which is seen in the data.

This thermal energy leakage away from the laser heated region heats the remainder of the sample. The temperature controller senses the increase in the sample temperature and tries to maintain the sample at a constant temperature. The heat diffusing away from the sample results in the temperature controller attempting to cool the bulk sample. This is seen when the laser is shut off at 300 °C and the temperature of the heating system drops by 0.5 °C in a few seconds. This effect is small but does reduce the temperature of the laser heated spot.

The result for the thermal conductivity of silicon at each of the three temperatures stated above agrees with published values. The values are all within uncertainty of published results, yet are consistently high. This leads to the conclusion that there are systematic errors in the results. One possible source of error is the overestimation of the amount of incident laser power absorbed by the sample. If less incident laser power is absorbed than theoretically predicted, the calculated thermal conductivity would have been higher. This could result from a thin silicon oxide layer that has grown on the surface of the silicon sample. The sample could have been slightly dirty, as well as surface roughness may have scattered some of the incident light as opposed to absorbing it.

The silicon sample was also in contact with the copper heating head at all times. Some of the heat deposited inside of the laser heated spot may have diffused into the copper, reducing the heating caused by the laser. The solution to the heat equation

derived in Chapter 4 assumed that this type of heat loss is negligible. The silicon being in contact with copper, a material with a very high thermal conductivity, did not completely satisfy this assumption. This was shown by the way the temperature controller measured a 0.5 °C drop in temperature when the laser was turned off.

The assumption of constant thermal conductivity and reflectivity for silicon through the range of temperatures induced during the heating is also suspect. During the trial with bulk silicon at 300 °C, the final temperature of the laser heated spot was 360 °C. The thermal conductivity would have decreased by 11 %, through this range and the reflectivity increased by 4%. Both of these factors would have led to an underestimation in the calculated thermal conductivity.

Another possible factor is thermally induced strain gradients inside of the heated material. Upon heating a material with the laser beam, the material directly in the path of the laser thermally expands, causing a strain gradient and compressive stresses within the sample. The formula for this stress is

$$\sigma = stress = EkT\,, \tag{8.1}$$

with σ being the stress, E being Young's modulus, k the coefficient of elasticity, and T the temperature increase.

Imaging the worse case possible for the experiment performed, the maximum induced heating was 60 K. Assuming that the entire beam spot is at this temperature, the thermally induced stress caused by the expansion of the silicon is :

$$\sigma = (47GPa)(2.6\times10^{-6}\,\mu m/m\bullet K)(60K) = 7.3\times10^{6}\,Pa\,. \tag{8.2}$$

According to F.H. Pollak and M. Cardona,[40] the largest measured stress induced Raman shift of silicon is 3.9 x 10^{-9} cm^{-1}/Pa. This would lead to a worse case strain

gradient induced Raman shift of 0.029 cm^{-1}. For the observed heating of 60K, the Raman shift was 1.8 cm^{-1}, and thermal strain gradients would cause an error of 1.5%. Since this is a first attempt at validating the all optical thermal conductivity measurement, and the error is relatively small, thermally induced strain gradients were neglected.

Photoelastic effects are also considered. The thermally-induced stress and strain can cause birefringence in a material. Light incident on the material would experience two different indices of refraction inside of the material. This would affect the reflectivity of the sample and the amount of absorbed laser light. This effect is believed to be negligible. Since the stress was shown to be small, the change in the index of refraction is also believed to be small. It would take a very large change in the index of refraction for a noticeable difference in the reflectivity. For theses reasons photoelastic effects have been neglected.

The thermal conductivity of GaS at 23 °C was measured as 87 +/- 12 W/m K, nearly one order of magnitude higher than the published value of 10 W/ m K. This can be attributed to the fact that the GaS sample had significant surface roughness. GaS has a layered structure, and the sample used was a platelet. When placed on the glass slide, the material would not lie flat, and folds and crevices in the material were clearly visible when the material was viewed with the naked eye. With higher surface roughness, more light was scattered off of the surface of the sample. For good coupling between the surface and the incident laser light, normal incidence onto the sample is needed. The high roughness of the gallium sulfide surface resulted in poor coupling between the laser light and the bulk sample. This reduced the absorbed laser light, and according to Equation 4.30 decreased the calculated thermal conductivity.

Another possible explanation for the high thermal conductivity is that gallium sulfide is a layered structure, and it exhibits anisotropic thermal conductivity. The assumption made in deriving Equation 4.30 was that the surface of the laser heated material remained the same size as the laser spot, and the heat diffused inward. This implied that the heat was transported away by the thermal conductivity in the direction parallel to the incident laser light, and that was the thermal conductivity believed to be measured in this experiment. That direction is the direction normal to the crystal sheets, referred to as parallel to the principal axis of the hexagonal GaS crystal in the literature. Since a thin plate film was used, the direction normal to the plate was also normal to the crystal layered structure.

The thermal conductivity in the parallel crystal direction for gallium sulfide is 10 W / m K.[36] In the perpendicular direction the thermal conductivity is 105 W / m K.[36] The experimental results appear to show that a large amount of the absorbed laser energy was transported away from the laser spot by the perpendicular thermal conductivity. This heat leakage reduced the temperature increase and increased the measured the calculated thermal conductivity. The measured thermal conductivity of gallium sulfide, 87 +/- 12 W/m K, is between the values of the parallel and perpendicular thermal conductivity.

The beam spot is measured by fitting it with a Gaussian curve. This was fitted in Origin, as shown in Figure 7.5. The fit is quite good with a reduced χ^2 value of 0.97, and the beam spot looked uniform. The beam waist was defined as $1/e^2$ of the peak intensity in the derivation of Equation 4.30, and with this criterion the beam diameter was 16 +/- 2 μm. The uncertainty in the beam diameter was determined by fitting different profiles of

the beam spot image and determining the variation in the values. The beam diameter was the greatest source of uncertainty the thermal conductivity calculation.

The temperature regulation was generally good at temperatures of 200 °C and above, but not very stable below these temperatures. At 200 °C and above, the temperature would stabilize within 0.1 °C, while at 100 °C the temperature would fluctuate within a band of 2 °C to 5 °C. This is a problem of tuning. The conditions for the heating chamber at 200 °C and above are different than the conditions below this temperature. The heat losses at the higher temperatures are greater and reduce overshooting, which allows the chamber to come to equilibrium faster. At lower temperatures, the vacuum chamber requires a long time to compensate for overshoot, and the chamber never reaches equilibrium. This problem can be overcome by properly tuning the chamber to two different settings, one set of parameters to be used for temperatures above 200 °C, and one for temperatures below 200 °C. The temperature control can be improved by auto tuning the controller every time a new vacuum is established in the chamber. The temperature accuracy for the Omega heating controller with a K thermocouple is stated at 0.4 °C. For absolute measurements of temperature this would be a systematic uncertainty, yet for relative temperature measurements such as the ones conducted in this thesis it is not.

8.3 Discussion of Possible Improvements to the Experiment

The experiment can be improved several ways. A limitation of the experimental set-up is that the probing laser is also the heating laser. The signal-to-noise ratios of the Raman spectra are dependent on the intensity of the probing laser. With only one laser

the signal-to-noise ratio changes depending on the amount of laser heating performed. An improvement on this is to incorporate two lasers, a heating laser and a separate probing laser, at two different wavelengths. The probing laser would remain at a constant low power and the heating laser intensity would vary.

The intensity of the Raman light depends to the forth power on the frequency of the incident laser light. The lower the frequency, the more intense should the Raman signal be. The experiment can be improved by using a 488 nm laser as the probing frequency for Raman spectroscopy. The heating can be performed with laser light frequency nearer to the infrared as to not interfere with the Raman signal. Incorporating a tunable laser would lead to the possibility of increasing the Raman signal intensity by performing resonant Raman spectroscopy, if possible for a chosen sample.

A CCD camera with a larger dynamic range can be used to measure the beam spot. This would lead to longer exposures being possible with the CCD and thus better time averaging of the signal. The beam spot could be fit with a three dimensional Gaussian peak to achieve a beam diameter with a better defined uncertainty.

One other major improvement could occur if there was less thermal leakage away from the laser heated sample area. This could be accomplished by using thinner samples as to not allow the heat to diffuse to the copper heating head during the experiment. Less thermal contact between the high thermal conductivity heating heat and the sample would improve the situation. If the Raman signal were intense enough, less heating power could be used. A smaller temperature rise at the heating spot would result in less thermal leakage, as well as better justify the assumption of constant thermal conductivity throughout the range of heating temperatures.

Another improvement is to measure the reflectance of samples directly as opposed to relying on published values. This will eliminate one source of possible systematic error in the experiment. The measurement could be performed once on the sample before its thermal conductivity is measured. Reflectance measurement techniques are beyond the scope of this thesis.

The experiment has a fundamental limitation based on the samples used. Currently, for the all optical thermal conductivity measurement method we have developed to work, the sample needs to have an optical signal that is sensitive to changes in temperature. It can be a photoluminescence or a Raman signal that changes with temperature, and this change must be large enough to give an accurate temperature measurement. The sample must also undergo heating by laser light. Not all possible choices of samples exhibit these characteristics. The usefulness of the experiment may be extended to samples that do not have these characteristics by coating unsuitable samples with very thin layers of laser absorbing materials to aid in heating or Raman active materials to allow an optical temperature measurement to be made. Although this would complicate the mathematics of the experimental calculations, it may still be possible to extract useful information about the thermal conductivity of the desired samples.

8.4 Extreme Condition Thermal Conductivity Measurement

To perform the all optical thermal conductivity measurement at high pressures, as it is our ultimate goal, several modifications to the experiment setup must be accomplished. To achieve the desired pressure a diamond anvil cell is needed. A diamond anvil cell is constructed by trimming the point of a brilliant cut diamond, resulting in a

flat terminal area referred to as a culet. Two of these trimmed diamonds are positioned so that a sample can be placed between their culets, as shown in Figure 8.1.

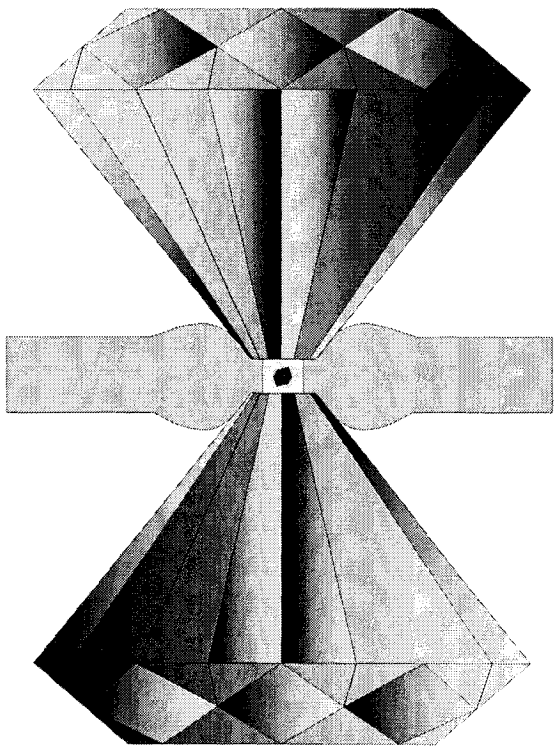

Figure 8.1: The Diamond Anvil Cell. The central small cube is the sample, the multi-toned materials are the diamond, and the light, single-toned material is the metallic gasket which constraints the sample between two diamond anvils.[41]

The first modification is that the diamond anvil cell must be incorporated into the setup. This will require that the working length of the objectives used be long enough to focus the laser beam spot onto the sample inside the diamond anvil cell. Determining the amount of light incident on the sample would no longer be a simple measurement. It is unknown how much of the light will hit the sample as the light must travel through the front diamond before hitting the sample. The front diamond must be characterized to determine how much of the incident laser light is reflected/absorbed by the diamond and

how much is incident on the sample. This can be done by sending laser light through only the front diamond of the anvil and measuring the amount of light transmitted. The beam spot inside of the diamond anvil must be measured. The beam spot must be imaged before and after going through the front diamond to see if there is any beam spot distortion.

Diamonds also have a very strong Raman signal and fluorescence. These will cause a background that will limit the samples that are possible to investigate. The Raman shift of diamond is centered at 1331 cm^{-1} at room temperature and is stress shifted to higher wavenumbers. Consequently its strong signal may make any Raman shifts between 1250 cm^{-1} and 1500 cm^{-1} unusable. The Raman light and fluorescence of diamond must be reduced from the light signal before any meaningful measurements can be made.

A final problem with the diamond anvil cell is that the sample will be in contact with diamond, the material with the largest thermal conductivity known. The sample inside of the diamond anvil cell will also have to be very small. These two details combined lead to the possibility that most of the heat absorbed by the sample will be transported away from the laser heated spot. This can lead to little or no detectable heating of the sample. This can be reduced by having the smallest laser spot possible and sending a large amount of laser intensity into the cell, thus inducing the largest temperature rise possible. The sample would have to be thermally insulated from the diamonds. Methods for doing this may be to coat all but one region of the sample with an insulating material, or to surround it in a pressure transmitting, low thermal conductivity medium.

Although there are some issues to overcome in applying the all optical thermal conductivity measurement to the diamond anvil cell, these difficulties are surmountable. The problems of large background signals, small samples and complications in sample heating are experimental difficulties commonly solved by physicists. Beyond the need for a more powerful laser source, better optics, and characterized diamonds, no fundamental problems exist with extending this measurement technique to extreme temperatures and pressures.

Chapter 9 : Conclusion and Future Work

9.1 Summary of Results

The experimental results of Périchon *et al.*[2], 125 K of surface heating under their experimental setup, have been verified against the theoretical calculations of Moody *et al.*[20] and Nissim *et al.*[22] The Raman shift's temperature dependence for silicon was measured as -0.024 ± 0.002 cm^{-1} per K, and that of gallium sulfide was measured as -0.026 ± 0.001 cm^{-1} per K. The thermal conductivity of silicon was measured as 175 ± 31 W/m K at 23 ± 1 °C, within uncertainty of the published value of 150 W/m K; 104 ± 24 W/m K at 200 °C , within uncertainty of the published value of 80 W/m K; and 79 ± 18 W/m K at 300 °C, within uncertainty of the published value of 63 W/m K. The thermal conductivity of gallium sulfide at 23 ± 1 °C was measured as 87 ± 12 W/m K, which is between the published values of 10 W/m K and 105 W/m K.

The specific goals for this thesis stated in the introduction have been accomplished. An all optical thermal conductivity measurement was designed and performed on test materials. The Raman shift's temperature dependence of silicon and gallium sulfide have been measured. The useful of the method was proven by measuring the correct thermal conductivity of silicon at 23 °C, and at higher temperatures of 200 °C and 300 °C, as well as gallium sulfide at 23 °C. The all optical thermal conductivity measurement was proven a success. The applicability of this method to high pressures was studied and found that with a few modification and improvements to the apparatus the experiment is feasible for research at high temperatures and pressures.

9.2 Possible Future Work in the Field

This project can also be extended to include the diamond anvil cell in the experimental setup. This allows the opportunity to subject the sample to high temperatures and pressures. This way, the thermal conductivity of geomaterials at extreme temperatures and pressures can be investigated.

[1] Air Products Inc. : http://www.airproducts.com/Products/fastfacts/charts_n_tables/definitions.asp (2006)
[2] S. Périchon, V. Lysenko, B. Remaki, and D. Barbier. "Measurement of porous silicon thermal conductivity by micro-Raman scattering", Journal Of Applied Physics, Vol. 86, No. 8, p. 4700 (1999)
[3] F. A. McDonald and G.C. Wetsel. "Photothermal and Photoacoustic Effects in Condensed Matter", Physical Acoustic, Vol. 18 , p. 167 (1988)
[4] M. Lax. "Temperature rise induced by a laser beam", Journal of Applied Physics, Vol. 48, No. 9, p. 3919 (1977)
[5] H. E. Cline and T. R. Anthony . "Heat treating and melting with a scanning laser or electron beam", Journal of Applied Physics, Vol. 48, No. 9, p. 3895 (1977)
[6] C. Kittel, Introduction to Solid State Physics. ©John Wiley & Sons, Inc. Toronto, 1986.
[7] N.W. Ashcroft and N.D Merman, Solid State Physics. ©Sanders College Publishing, New York, 1976.
[8] S. Gasiorowicz, Quantum Physics. ©John Wiley & Sons, Inc., New York, 2003
[9] R. M. Besancon, The Encyclopedia of Physics ©Reinhold Publishing, New York, 1966.
[10] P. N. Butcher and D. Cotter, The Elements of Nonlinear Optics. ©Cambridge Uniersity Press, Cambridge, 1990.
[11] L. S. Pedrotti and F. L. Pedrotti, Optics and Vision. Prentice Hall, New Jersey, 1998.
[12] W. Lauterborn and T. Kurz, Coherent Optics. Springer, New York, 1993.
[13] R.C. Denney, A dictionary of spectroscopy. ©The Macmillan Press, New York, 1973.
[14] H.E. Hall, Solid state physics. ©John Wiley & Sons, Inc., New York, 1974.
[15] Shuibo, Xie, Iglesia. "Effects of temperature on the Raman Spectra and Dispersed Oxides", Physical Review B, Vol. 3, No. 12, p. 5144 (1971)
[16] M. Giehler, M. Ramsteiner, P. Waltereit, O. Brandt, K.H. Ploog, and H. Obloh "Anharmonicity of the E2(high) and A1(LO) phonons in GaN studied by temperature dependent Raman spectroscopy", Physica B : Condensed Matter, Vol 316, p. 162 (2002)
[17] J.F Mammone and M. Nicol. "Raman Spectra of TiO_2-II, TiO_2-III, SnO_2, and GeO_2 at high Pressure", Journal of Physical Chemistry : Solids, Vol. 42, p. 379 (1981).
[18] A. Iqbal. "Temperature dependence of Raman-active phonons and nature of the phase transition in lithium and sodium azide", The Journal of Chemical Physics, Vol. 59, No. 4, p. 1769 (1973)
[19] J.B. Cui, K. Amtmann, J. Ristein. " Noncontact temperature measurements of Diamond by Raman Scattering Spectroscopy", Journal of Applied Physics, Vol. 83, No. 12, p. 7929 (1998)
[20] J.E. Moody and R.H. Hendel. "Temperature profiles induced by a scanning cw laser beam", Journal of Applied Physics, Vol. 53, No. 6 p. 4364 (1982)
[21] Edward D. Palik, Handbook of optical constants of solids. © Academic Press Inc., 1985.
[22] Y.I Nissim, A. Lietoila, R.B. Gold and J.F. Gibbons. "Temperature distribution produced in semiconductors by a scanning elliptical or circular cw laser beam", Journal of Applied Physics, Vol. 51, No. 1, p. 274 (1980)
[23] Lexel Laser Inc. Model 95 Ion Laser Manual. ©Lexel Laser Inc, Fremont, California, 1984.
[24] Newport Spectra-Physics Division : http://www.newport.com/Centennia-Thin-Disk-Laser/474031/1033/catalog.aspx (2006)
[25] Thorlabs Inc. : http://www.thorlabs.com/ (2006)
[26] Thorlabs Inc. : http://www.radians.se/thorcat/4200/4242-s01.pdf (2005)
[27] Typical data from Semrock Inc. : http://www.semrock.com/Catalog/MaxLine_spectra.htm (2006)
[28] Typical data from Semrock Inc. : http://www.semrock.com/Catalog/RamanEdgeFilter_spectra.htm (2006)
[29] Jobin Yvon Inc. : http://www.jobinyvon.com/Spain/esdivisions/OSD/currentmonos.htm (2006)
[30] Abra Electronics Corp. : http://www.abra-electronics.com/catalog/chemicals/gc27.html (2006)
[31] Omega Engineering Inc. : http://www.omega.com/temperature/tsc.html (2001)
[32] McMaster-Carr : http://www.mcmaster.com/ (2006)
[33] Omega Engineering Inc. : http://www.omega.com/pptst/CNI_Series.html (2001)
[34] DuPont Teijin Films. https://192.168.0.239/filmenterprise/backup/datasheet%2Dmetric.asp (2005)
[35] M.A. Alzahdanov, M.D. Nadzahafzade and Z. Yu. Seidov. "Thermal conductivity of gallium sulfide", Physics of the Solid State, Vol. 41, No. 1, p. 20 (1999)

[36] S. Desgreniers, K. Lagarec. "XRDA: a program for energy-dispersive X-ray diffraction analysis on a PC", Journal of Applied Crystallography, Vol. 27, No. 3, p.432 (1994)
[37] R. Loudon, The quantum theory of light. ©Clarendon Press, Oxford, 1973
[38] Origin 7.5 SR4. © OriginLab Corporation, Northampton, MA, 2004.
[39] P. Jenkins, M. Tuma, and D. Naghski. "Optical Constants of thin film gallium sulfide layers", The International Society for Optical Engineering, Vol. 2686, p. 115 (1996)
[40] F.H. Pollak, M. Cardona, E. Anastassakis, A. Pinczuk, and E. Burstein. "Effects of static uniaxial stress on the Raman spectrum of silicon", Solid State Communications, Vol. 8, No. 2, p. 133 (1970)
[41] S. Desgreniers, May 16, 2006, obtained through personal communications